MODELING OF BLADE CUTTING OF VISCOELASTIC BIOMATERIALS

A DISSERTATION
SUBMITTED TO THE FACULTY OF THE GRADUATE SCHOOL OF THE
UNIVERSITY OF MINNESOTA
BY

Yun Peng

IN PARTIAL FULFILLMENT OF THE REQUIREMENT FOR
DEGREE OF MASTER OF SCIENCE

ADVISED BY
Dr. Debao Zhou

June 2013

ACKNOWLEDGEMENTS

I would like to express my deepest appreciation to all those who provided me the possibility to complete this report. I owe my special gratitude to Dr. Debao Zhou, who is the supervisor of my master's degree in UMD, for his trust, instructions, patience and encouragement. It's a memorable and fruitful two years working with him.

Furthermore I would like to acknowledge Dr. Ryan Rosandich and Dr. Mohammed Hasan for serving on my thesis committee. I thank Dr. Ryan Rosandich for his support to my career in UMD. I thank Dr. Robert Feyen and Dr. Nathan Johnson for their recommendations to my Ph.D. applications. I thank all the faculties and staffs who once taught in classes and whom I once worked with. They made my life in UMD most wonderful.

I am so grateful to have the supports from my parents, for their unconditional love, great trusts and encouragements. I am also so grateful to have so many good friends for their accompaniment during these two years.

At last, I owe my great appreciations to my dear girlfriend Tiantian Zhang: you are my strongest motivation to strive for a better future.

DEDICATION

This dissertation is dedicated to my parents.

For your everlasting love.

ABSTRACT

The work in this thesis focuses on the modeling of blade cutting of viscoelastic materials. The blade cutting procedure is modeled in two stages. The first stage is the contact of the blade with the cutting material and the second stage is the fracture during continuous cutting. The modeling of the first stage is used to predict the initiation of the cutting fracture and the modeling of the second stage is use to characterize the cutting force during continuous fracture. Experiments that are used to determine the material parameters for the simulations and calculations of the cutting process are also carried out.

The first stage is modeled as the area contact between the edge of the blade and cutting materials. It is modeled by applying the elastic-viscoelastic correspondence principle to the solutions for point load and then by performing a numerical integration scheme to extend the solutions to distributed pressure cases. The stress tensor was analytically obtained at any given point inside the viscoelastic material. The effect of slicing angles on the stress distribution is then evaluated. Using the principal stresses, the location of damage is predicted using Tresca's failure criterion. In the continuous damage stage, FEM simulation using ABAQUS is used as the modeling method. A bi-layered structure is applied to represent the tissue-bone structure which could be widely seen in a deboning process. In the simulation, the cutting force is monitored during the blade cuts through the interface. The dynamic change of the force pattern when the blade approaches the interface is analyzed in order to propose a control algorithm that prevents

the blade cutting into bones. In order to provide realistic data for the simulation, several relaxation tests are designed to obtain the tensile relaxation modulus for biomaterials. Ligaments obtained from chicken wings and legs are used as specimens. The experimental data was theoretically fitted into a Burgers Model for the simulation and calculation.

The model developed in this research can serve as a guideline for many applications such as the design of a surgical simulator to facilitate the training of new doctors and the intelligent control of a robot for deboning process to improve cutting yield and meat harvesting quality.

TABLE OF CONTENTS

CHAPTER I INTRODUCTION

1.1 Background

Biomaterials have been studied since antiquity. However, their development booms in very recent decades, mostly due to practical needs especially in medical and clinical applications. Today, biomaterials are taking part more and more in research and clinical operations such as joint replacements, bone plates, artificial ligaments and tendons, heart valves, and so on. The large demand for biomaterials in various uses has inevitably called for the knowledge of its properties in mechanics, chemistry and biology. The study of biomaterials aims to provide a deep understanding of their mechanical and chemical properties and to advance their applications in various disciplines.

With the development of material science, Hooke's Law can never suit for the practical use. Most materials demonstrate complex mechanical behaviors such as: non-linear stress-strain relationship, plasticity, fracture and failure and time-dependence, especially for biomaterials, such as polymer or soft biological tissues. Among these properties, viscoelasticity is an important but also intriguing one. Common materials will show either solid or fluid properties; in other words, the stress either depends on the immediate amount of strain or on the immediate rate of the strain. However, viscoelasticity shows the combination of both and thus cannot be only described by either elasticity or viscosity theory.

Materials which fall into that range have a memory for all past states, and thus, the current stress depends upon the entire history of deformation. The study of viscoelasticity also receives a fast development in recent decades mostly due to the vast application of polymer materials. Research of biomaterials benefits a lot from the development of viscoelastic theory.

Though the viscoelastic theory provides a great knowledge of the mechanical properties of biomaterials, it is still an ideal abstraction of the real material property in some degree. The non-linearity is the biggest bottleneck problem for researchers, and therefore, many methods have been raised to address this issue. One of the most famous methods is to combine the hyperelastic theory, which describes non-linear elastic mechanical behavior, with viscoelastic theory, yielding the visco-hyperelastic theory. This visco-hyperelastic theory in a large degree solves researchers' problems, and it has been proven to be especially useful in numerical methods such as the finite element method. It provides a convenient connection to some FEM software such ABAQUS and thus is largely welcomed by researchers. Besides, theory of viscoplasticity was also raised to describe the plastic behaviors of many biomaterials. Fracture and failure analysis were also carried out on biomaterials. Thanks to the development in these theories, the application of theoretical models to real life is much easier.

With the tools in hand, applications, especially in medical or clinical research, could be carried out. Various biomechanical applications such as the joint replacement or artificial heart valve rely on these studies. Among numerous applications, the contact problem is the most fundamental but also significant one. Contact problems are nearly everywhere in clinical or medical applications. The simplest case is the operation using a

scalpel. Physicians want to precisely cut the object with no extra damage to other tissues. The contact of the blade and the tissue is a typical contact problem. The difference between soft tissues in mechanical properties makes the precise cutting possible; however, without vast clinical experiences, it is an extremely difficult task for a new physician to accomplish such a task. Standing from a mechanical engineer's perspective, it would be very helpful if such equipment, which could mimic the dynamic feelings of the scalpel during cutting in different materials to the operator's hand, is available. It's not a groundless imagination. With the knowledge in biomaterial science, viscoelasticity and contact problems, it is completely reasonable to realize such a tool.

Similar examples also exist in the food processing industry. The large market demands of boneless meat products make food processing companies hire a large number of workers to perform the deboning tasks, such as dissecting meats from chicken breasts. The deboning process requires a lot of skills in manipulating the blade, and is also a highly repetitive task, which is very likely to cause muscle fatigues to workers. On the other hand, muscle fatigue would cause imprecise control over the blade and thus would not only harm the workers' health, but also lower the product yield rate (cutting too shallow so that a lot of meat is wasted) and quality (cutting too deep to the bone so that bone chips exist). Robotic-controlled machines could be a potential solution to such a deboning process dilemma. By monitoring the blade force pattern change when the blade approaches the interface between the meat and bone and teaching the computer, it is possible to let the robot continue cutting until a signal indicates that the bone is very close so that the cut will be deep enough to maximize the yield rate and also not too deep to cut into the bone to keep the product from bone chips.

1.2 Motivation

All these practical needs have inevitably called for the researchers to dig into the contact and continuous cutting of a viscoelastic biomaterial, and thus here yields this research. With many possible thrusts, this research focuses on the efficiency of the cutting process of a biomaterial which demonstrates viscoelasticity. More specifically, the cutting effectiveness is examined through the analysis of the stress distributions under different cutting angles. Useful guidelines for applications, in which prevention or improvement in cutting effectiveness is concerned, are expected.

1.3 Scope

The models developed in this research aim to simulate a complete cutting process in a viscoelastic solid. Analytic solutions to the stress fields were derived in the blade-body contact model and were used to simulate the initial pre-rupture stage. The FEM model by ABAQUS was performed to simulate the continuous cutting stage. The models could be used in many applications such as surgical simulator designs or deboning robot designs. The experimental work carried out included the tensile relaxation test which determines the viscoelastic properties of the linear isotropic homogenous viscoelastic materials.

The thesis is arranged as follows: Chapter II covers a literature review on viscoelastic contact problems; Chapter III describes the modeling of the whole cutting process which includes the fundamental theories of viscoelasticity, the analytic modeling of stage I: contact between a blade and a viscoelastic body, and the FEM modeling of

stage II: continuous cutting process. The experimental set-up which provides the essential parameters for Chapter III is presented in Chapter IV. All the results are presented in Chapter V. Conclusions are reached and future recommendations of this research are offered in Chapter VI. In Appendix, the MATLAB codes for the numerical strategies for calculating the stress components as introduced in Chapter III are provided.

CHAPTER II REVIEW OF LITERATURE

The purpose of this chapter is to provide a basis for this study by reviewing literature that is pertinent to the goals and objectives of this research. The topics of literature reviews are the contact problem, viscoelastic modeling and fracture analysis of biomaterials.

2.1 Contact Problem

Many researchers investigated the contact problem in which a half-space is subjected to loads on the free surface. Early studies on contact problems could date back to 19th century. Boussinesq (1885) considered the problem of a concentrated force on the half-space in his paper in 1885. Cerruti (1882) obtained the solutions by use of singularities from potential theory. In solving these two classic problems, the half-space medium was assumed to be isotropic, homogeneous and elastic.

Since Boussinesq and Cerruti's work, a number of researchers have tried to develop these problems in different ways. One direction was to apply these two basic solutions to cases where loading conditions are over a certain geometrically simple regions. In these cases, the solution could be constructed via superposition. Love (1929) provided the integral for a rectangular and circular area with constant normal pressure.

Dydo and Busby (1995) completed the solution for first order polynomial load applied to rectangular surface. The stress and deformation produced by a pressure distribution of the form $P_0\sqrt{1-x^2/a^2}$ acting on the rectangle x [-a,+a], y [-b,+b] have been calculated by Kunert (as described in Johnson(1985)). The explicit solution for normal deflection due to a polynomial distribution of normal pressure acting on a triangular region has been given by Svec and Gladwell (1971). Li and Berger (2001) derived all the solutions for the problem under a combined loading which include both normal pressure and tangential stress, namely the Boussinesq-Cerruti problem, with various loading profiles including constant, linear and bilinear distributions over a triangle area. Based on the theoretical solutions, a numerical approach was also given with friction considered (Li and Berger 2003). Schepers, Savidis and Kausel (2010) extended the classic solutions to dynamic loads with an application in geotechnical studies. The stress components were presented using pressure bulbs on given planes.

Another direction is to consider the classic solutions for viscoelastic medium. Talybly (2010) studied the problem on the action of a normal concentrated force on the surface of viscoelastic half-space, namely, Boussinesq's viscoelastic problem. The relationship of the theory of linear isotropic viscoelasticity was used as determining relations. Peng and Zhou (2012) derived the solutions for the viscoelastic half-space problem under a concentrated tangential force, namely Cerruti's viscoelastic problem, and formulated the solution for a general case in which both tangential and normal forces are applied. The solution could be used to predict the stress distribution in the initial step of blade cutting problems. Adolph et al. (2007) evaluated the solution for a 3D isotropic, viscoelastic half-space subjected to vertical rectangular surface stress loading of constant

amplitude using the Radon and Fourier transforms. The inverse transform which was essential for viscoelastic solution was performed numerically. There were also some other viscoelastic half-space problem solved in which the loads were applied in the medium (Piombo, Tallarico and Dragoni, 2007), but these problems did not fall into the category.

Though quite a number of researches were extended from the classic Boussinesq's and Cerruti's problem, none of them provided a thorough study on a case which simultaneously addressed all the following factors: 1) considers the surface loading, 2) considers a non-constant loading profile,3) considers a combined loading condition and 4) considers the problem in a viscoelastic medium. However, such a complete study was very necessary because it comprises the base for studies on contact problems with biomaterial applications. For example, in the food processing industry, it is desired to know the stress distribution in a food medium (potato or meat) under a robot-controlled blade cut into the food surface. Or in clinical operations, the stress distribution inside an organ (e.g. liver or kidney) under certain scalpel operations is very crucial. The model of both applications requires all four aspects as above mentioned. This study aims to provide a thorough investigation into such a problem and strives to link the theoretical solutions to applications. Specifically, the purpose of this research is to solve the stress and displacement fields of a viscoelastic half-space subjected to any arbitrarily defined loading profile on the free surface.

2.2 Viscoelasticity Modeling

The viscoelastic property of the medium inevitably leads the problem to a step of defining the viscoelasticity. The mechanical response of viscoelastic materials to mechanical excitation has traditionally been modeled in terms of elastic and viscous components such as springs and dashpots. The corresponding theory is analogous to the electric theory, which is extensively described in engineering textbooks. Typically used models are Maxwell's model, Kelvin-Voigt model, Standard Linear Solid model and Burgers model (Lakes, 1999, p23-30). The generalized Maxwell model is the most general form of the linear model for viscoelasticity. It takes into account that the relaxation does not occur at a single time but at a distribution of times. All the previous models could be viewed as particular cases of generalized Maxwell mode. Viscoelastic modeling is important for biomaterial research because both theoretical calculation and numerical simulation call for the modeling parameters. Many researchers have investigated the modeling problem for biological tissues and provided a directly useable method to the problem addressed in this study.

Zhang, Chen and Kassab (2007) investigated the rate-insensitive feature of biological materials by a generalized Maxwell model. A geometric series was used to minimize the number of model parameters. The model shows good fit of experimental relaxation data. Masakatsu, Toshio, Shin, Zhang and Kanako (2007) used Burger's model to fit experimental data obtained from fetal rat tissues. Burger's model was also used to determine the effective behavior of a microcracked linear viscoelastic solid. (Nguyen and Dormieux, 2011)

When the mechanical response cannot be assumed linear, the hyperelastic strain energy density could be introduced to account for the stress-strain response. Viscoelastic models could still be used. Snedeker, Barbezat, Niederer, Schmidlin and Farshad (2005) designed an impact experiment to study the rupture behavior of a kidney. The second-order hyperelastic Mooney-Rivlin material with viscoelastic behavior implemented via a second-order Prony series was introduced to characterize the mechanical behavior of renal tissues. In this study, a simple exponential decaying function is assumed for the viscoelastic bulk and shear modulus.

Many researchers have investigated the viscoelasticity of various biomaterials. Nasseri, Bilston and Phan-Thien (2002) studied the viscoelastic properties of pig kidney in shear and developed a multi-mode upper convected Maxwell model using experimental results. Geerligs, Peters, Ackermans, Oomens and Baaijens (2008) measured and described the linear viscoelastic behavior of subcutaneous adipose tissue. Abdel-Wahab, Alam and Silberschmidt (2011) analyzed the anisotropic viscoelastoplastic properties of cortical bone tissues. Kim, Lee and Kim (2010) determined the shear and bulk moduli of viscoelastic solids from the indirect tension creep test. Instead of only studying the viscoelastic shear modulus or elastic modulus, their study provided a method to obtain both of these two time-dependent mechanical properties, which was very helpful for the FEM implementation.

Cheng and Yang (2009) obtained the shear relaxation modulus and creep compliance of linear viscoelastic materials from instrumented indentation using axisymmetric indenters of power-law profiles. Valtorta and Mazza (2005) used a torsional resonator device to dynamically measure the soft tissue viscoelastic properties.

Zhang, Chen and Kassab (2007) developed a rate-insensitive linear viscoelastic model for soft tissues using a generalized Maxwell model. It's worthy to mention that the model used a geometric series for the frequencies of Maxwell elements so that the number of model parameters was minimized to five. Nguyen, Dormieux, Pape and Sanahuja (2011) developed a Burger Model for the effective behavior of a microcracked viscoelastic solid. The relationships among viscoelastic moduli were studied by Oza, Vanderby and Lakes (2006). They used a single-integral nonlinear superposition principle to relate creep and relaxation.

Many researchers carried out works to study the mechanical properties of ligaments and tendons, which are the most important components in human body motions. The understanding of their mechanical behavior would be a great help for research and clinical diagnosis. Pena, Pena and Doblare (2008) theoretically modeled the nonlinear viscoelastic effects of ligaments undergoing finite deformation. DeFrate and Li (2006) evaluated the ability of several models to predict the elastic stress response of ligament and tendon at strain levels higher than the levels used to fit the model. Pioletti and Rakotomanana (2000) developed an experimental method to test the hypothesis of variables separation that is widely used in soft tissue biomechanics.

The viscoelastic properties were vastly used in applications. Yamashita et al. (2008) designed a bending manipulator for fetoscopic intrauterine laser therapy to treat twin-to-twin transfusion syndrome. Dhar and Zu (2007) designed a resonator device for in vivo measurement of regional tissue viscoelasticity. The design had an advantage of being non-invasive and localized.

2.3 Fracture Modeling: Insertion and Slicing

An important biomaterial research thrust is the understanding of the continous damage process, which is ubiquitous in the food processing industry and in clinical operations. Modeling the damage models such as insertion or slicing would provide guidelines for these practical applications and thus improve the efficiency or reduce the risk. Therefore it is important to raise a suitable fracture criterion for the biomaterial undergoing large deformation. Subit, Chabrand and Masson (2009) developed a micromechanical model to predict damage and failure in ligament tissues, which is applied to the ligament-to-bone attachment in the human knee joint. Natali et al. (2008) developed a visco-hyperelastic-damage constitutive model for the analysis of the biomechanical response of the periodontal ligament. This model could include in both the non-linearity and time-dependent behavior of the soft tissues. Mann and Damron (2002) used a non-linear fracture mechanics approach to predict the failure response of complex cement-bone constructs with mechanical tests of tensile and shear loading performed. Gamonpilas, Charalambides and Williams (2009) investigated the large deformation and fracture properties of two types of starch gels (viscoelastic material) through uniaxial compression, single edge-notched bend and wire cutting experiments. Koop and Lewis (2003) developed a model to estimate the fracture energy and viscoelastic work for soft viscoelastic tissues.

Besides experimental studies, numerical methods were also used. Geubelle (1997) developed a numerical method for elastic and viscoelastic dynamic fracture problems in homogenous and biomaterial systems. The fracture tests were numerically performed on composites which demonstrate viscoelasticity as well. Cordes, Chang and Charvet (1998)

used a nonlinear finite element method to predict the maximum loads on pre-cracked panels and concluded that the predicted maximum loads were within the 6% of the experimental loads. Bouchbinder and Brener (2011) calculated the scaling properties of the quasi-static energy release rate and the viscoelastic contribution to the fracture energy of various biological composites using both perturbative and non-perturbative approaches.

Shergold and Fleck (2004) developed micromechanical models for the deep penetration of a soft solid by a flat-bottomed and by a sharp-tipped cylindrical punch. The soft solid is considered as an incompressible, hyperelastic, isotropic solid described by a one-term Ogden strain energy function. Mahvash and Dupont (2010) described the mechanics of the rupture events during needle-based procedures and analyzed the effect of insertion velocity on needle force, tissue deformation and needle work.

In this research, particular interests are given to the cutting/slicing process. Previous researches include: Atkins, Xu and Jeronimidis (2004) explained the reason why it is relatively difficult to cut when simply pressing down but much easier when there are sideways sawing or slicing actions. The model was developed using the energy based process. Kamyab, Chakrabarti and Williams (1998) described an analysis of cutting in terms of the fracture toughness, the yield stress and the coefficient of friction. Mahvash et al. (2008) presented an analytical model based on the concepts of contact mechanics and fracture mechanics to calculate forces applied to scissors during cutting of a slab of material. Though viscoelasticity was not considered in the cutting process, this research gave a good example of the energy relationships during a cutting process. Brown, James and Purnell (2004) designed cutting experiments to investigate the parameters affecting

cutting forces. Reyssat, Tallinen, Merrer and Mahadevan (2012) experimentally evaluated the cutting efficiency of slicing and squeezing, and concluded that the slicing motion leads to fracture nucleation with minimal deformation of the bulk and thus a much lower barrier. The cutting application in food processing was also investigated. Dempsey and McGorry (2004) investigated the force exertions during pork shoulder deboning.

2.4 Problem Summary

As a summary of this research, in stage I, *i.e.* the stage of contact, analytic solutions to the stress and displacement field of a contact problem will be obtained. In this stage, the body should be modeled as isotropic, homogenous and viscoelastic medium. An arbitrarily assigned combined loading condition should be applied on the free surface. In stage II, *i.e.* the stage of continuous cutting, the blade forces are to be obtained during a continuous cutting process in a bi-layered (soft tissue and bone) structure by ABAQUS. Relations to applications are expected. Experiments are also to be performed to provide numerical values for the parameters used to obtain the analytic and FEM results.

CHAPTER III MODELING THE CUTTING OF VISCOELASTIC MATERIALS

In this chapter, the formulation of the stress distribution within a viscoelastic material subjected to distributed pressure on the free surface is presented. The stress tensor at any point in the material is obtained with two steps. First, the elastic-viscoelastic correspondence principle is applied to obtain the stress solution for a viscoelastic material under a point load. Second, the obtained solutions from first step are integrated over the stress-applying area. Based on the formulation, the tress tensor at any point in the material is calculated numerically. This formulation can be used to simulate many practical contact problems where the stress field elicited is concerned. One important example could be the biomaterial cutting operations where a blade interacts with a biomaterial. In cutting, the effect of slicing angle on the stress distribution is an important factor to be included in the discussion. The slicing angle is determined by the magnitudes of tangential and normal components of the cutting force. Using the calculated principal stresses, it is possible to predict the location of damage using failure criteria such as Tresca's criterion. The results can serve as guidelines for applications where the stress distribution and fracture prediction in viscoelastic materials are concerned.

3.1 Introduction to Viscoelasticity

Viscoelasticity is one of the fundamental theories in this research, and therefore it is worthy to introduce its mathematic forms and meanings. A thorough introduction to these theories could be found in many textbooks of viscoelasticity, and the following contents are majorly from *Viscoelastic Solids* (Lakes, 1999).

Most engineering materials are described by Hooke's law for small strains: stress σ is proportional to strain ε. In one dimension, Hooke's law is as follows:

$$\sigma = E\varepsilon$$

with E denoting Young's modulus.

In contrast, a viscous fluid under shear stress obeys:

$$\sigma = \eta \frac{d\varepsilon}{dt}$$

with η denoting the viscosity.

Elastic materials strain when stretched and quickly return to their original state once the stress is removed. Viscous materials, like most liquid, resist shear flow and strain linearly with time when a stress is applied. Viscoelasticity is the property of materials that exhibit both viscous and elastic characteristics when undergoing deformation. Whereas elasticity is usually the result of bond stretching along crystallographic planes in an ordered solid, viscosity is the result of the diffusion of atoms or molecules inside an amorphous material.

The stress-strain relationship for viscoelastic materials depends on time. Some phenomena in viscoelastic materials are:

(a) If the stress is held constant, the strain increases with time. This is called *creep*.

(b) If the strain is held constant, the stress decreases with time. This is called *relaxation*.

(c) The effective stiffness depends on the rate of the applied load.

(d) If cyclic loading is applied, hysteresis (phase lag) occurs, leading to the dissipation of mechanical energy.

(e) Acoustic waves experience attenuation.

(f) Rebound of an object following an impact is less than 100%.

(g) During rolling, frictional resistance occurs.

3.1.1 Creep

When subjected to a step constant stress, viscoelastic materials experience a time-dependent increase in strain. This phenomenon is known as viscoelastic creep. In one dimension, suppose the history of stress σ to be a step function beginning at time zero:

$$\sigma(t) = \sigma_0 \mathrm{H}(t)$$

$H(t)$ is the unit Heaviside step function defined as 0 for time t less than zero, 1 for t greater than zero, and 0.5 for t =0. The strain $\varepsilon(\tau)$ in a viscoelastic material will increase with time. The ratio

$$J(t) = \frac{\varepsilon(t)}{\sigma_0}$$

is called the creep compliance.

As shown in Figure 3-1, at a time ($t = t_0$), a viscoelastic material is loaded with a constant stress that is maintained for a sufficiently long-time period to $t = t_1$. The material responds to the stress with a strain that increases until the material ultimately fails, if it is a viscoelastic liquid. If, on the other hand, it is a viscoelastic solid, it may or may not fail depending on the applied stress versus the material's ultimate resistance. When the stress

is maintained for a shorter time period from t_0 to t_1, the material undergoes an initial strain increase. At the moment when the stress immediately decreases to zero, the strain is then gradually decreases to a residual strain.

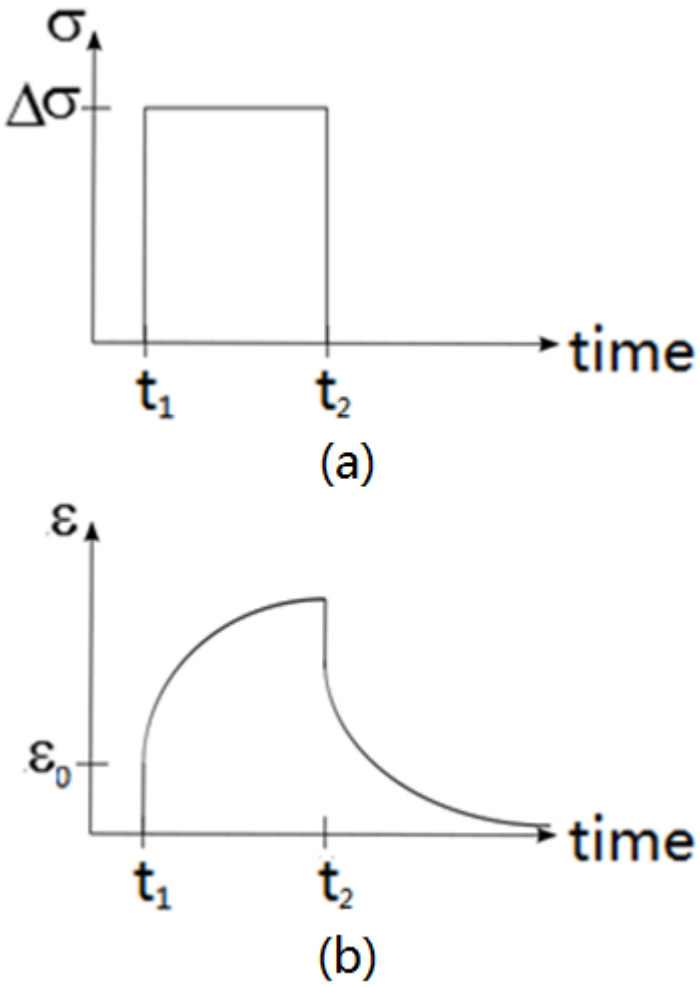

Figure 3.1 a) Applied stress and b) induced strain (b) as functions of time over a short period for a viscoelastic material.

Viscoelastic creep is important when considering long-term structural design. Given loading and temperature conditions, designers can choose materials that best suit component lifetimes.

3.1.2 Stress Relaxation

Stress relaxation is the gradual decrease of stress when the material is held at constant strain. If the strain history is a step function beginning at time zero:

$$\varepsilon(t) = \varepsilon_0 \mathrm{H}(t)$$

the stress $\sigma(t)$ in a viscoelastic material will decrease as shown in Figure 3.2. The ratio

$$E(t) = \frac{\sigma(t)}{\varepsilon_0}$$

is called the relaxation modulus.

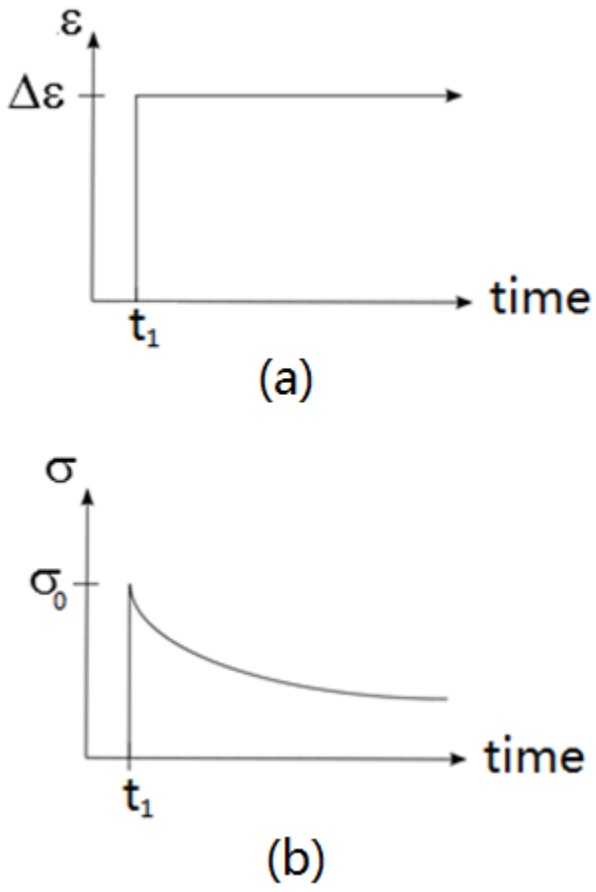

Figure 3.2 a) Applied strain and b) induced stress as functions of time for a viscoelastic material.

Creep and relaxation can occur in shear or in volumetric deformation as well. The relaxation function for shear is expressed as $G(t)$. For volumetric deformation, the elastic bulk modulus is expressed as $K(t)$.

3.1.3 Constitutive Relations

To predict the response of the material to any history of strain, constitutive equations are developed with Boltzmann superposition principle, which states that the effect of a compound cause is the sum of the effects of the individual causes. Consider an arbitrary history of strain $\varepsilon(t)$ as a function of time t as shown in Figure 3.3.

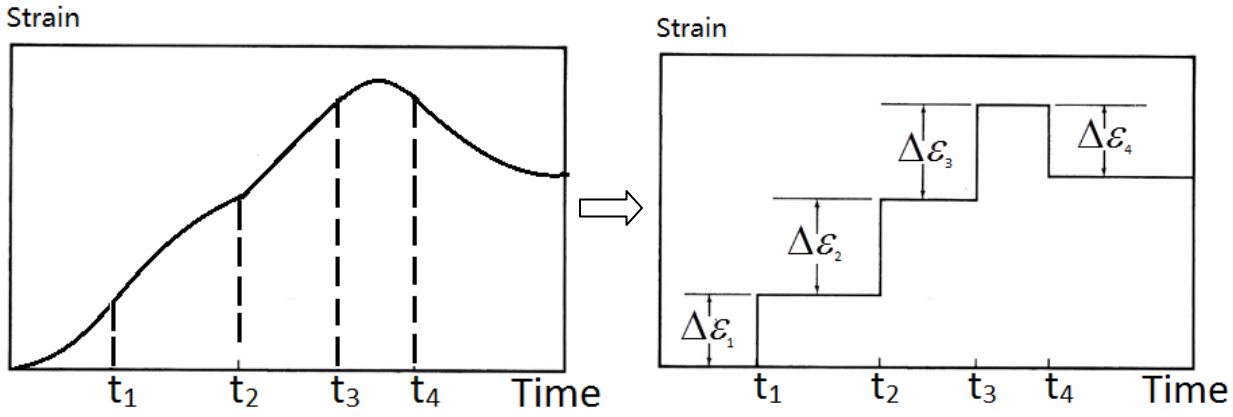

Figure 3.3 Analysis of arbitrary strain history: decomposition into pulse functions.

Consider a segment of this history from $t-\tau$ to time $t-\tau+\Delta\tau$, as shown in Figure 3.3. The segment of strain history may be written as

$$\varepsilon(t)=\varepsilon(\tau)\left[\mathrm{H}(t-\tau)-\mathrm{H}(t-\tau+\Delta\tau)\right].$$

From the Boltzmann superposition principle, the increment of stress at time t due to strain pulse in the past is:

$$\Delta\sigma(t) = \varepsilon(\tau)\left[E(t-\tau) - E(t-\tau+\Delta\tau)\right].$$

Since

$$\frac{dE(t-\tau)}{d\tau} = \lim_{\Delta\tau\to 0} \frac{E(t-\tau+\Delta\tau) - E(t-\tau)}{\Delta\tau},$$

the stress increment may be written

$$d\sigma(t) = -\varepsilon(\tau)\frac{dE(t-\tau)}{d\tau}d\tau.$$

The entire strain history may be decomposed into many of such pulses. The stress at time *t* is the summation of the stress effects of each of these pulses. In the limit as the pulse width $\Delta\tau$ becomes small, the summation converges to an integral:

$$\sigma(t) = \int_0^t E(t-\tau)\frac{d\varepsilon(\tau)}{d\tau}d\tau = \int_0^t E(t-\tau)d\varepsilon.$$

Similarly, for strain response with arbitrary stress history, the integral is:

$$\varepsilon(t) = \int_0^t J(t-\tau)\frac{d\sigma(\tau)}{d\tau}d\tau = \int_0^t J(t-\tau)d\sigma.$$

Note that in the above two integrals, σ□□□ and ε□□□ are assumed to be zero at t=0 so that the term containing the initial conditions do not appear in the right hand side of the integrals.

Consequently, if the response of a material to step stress or strain has been determined experimentally, the response to any load history can be obtained.

3.2 Stage I Modeling: Contact between Blade and Biomaterial

3.2.1 Model Description

The cutting material is considered as a viscoelastic semi-infinite solid with plane boundary. The interaction of the blade with bio-material is simplified as a rectangle area force acting on the upper surface of the viscoelastic semi-infinite solid as shown in Figure 3.4.

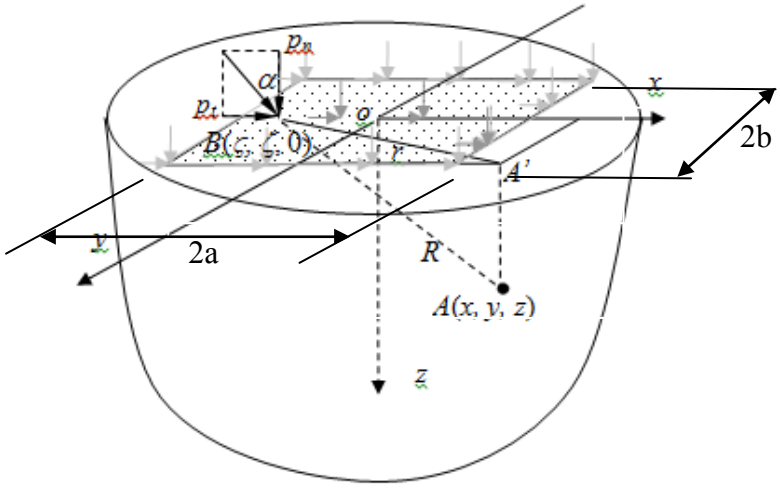

Figure 3.4 Half-space model for the cutting contact problem.

In the modeling of cutting, the contact of the blade with a bio-material is modeled as the cutting force with vertical and tangential distributed force components acting on the surface of the half-plane. The reason to select rectangular-area force is that the contact between the blade edge and the cutting material is an area rather than a line, since a very small cutting force will generate infinite stress if the contact between two objects is a line. The solid is considered as semi-half space since it is assumed that the cutting influence depth is much shorter than the depth of the solid. In Figure 3.4, frame *O-xyz* is fixed on the surface of the cutting edge. Point *O* is in the center of the contact area, point *A* is the point which we are interested in, and point *A*' is the projection of point *A* on the

O-xy plane. *x*-axis is along the blade length direction, *y*-axis is along cross-blade direction, *and z*-axis points into the material. *x-, y-* and *z*-axes follow the right-hand rule.

The cutting force P is applied with two components: P_n as the normal component along z direction (subscript n stands for normal direction) and P_t as the tangential component along x direction (subscript t stands for tangential direction). The angle between P and P_n is marked as α, called slicing angle. Noted is that the y direction component is not considered since there is no cutting force in y-axis direction. The contact area between the blade and the material is a rectangular region with $[-h, h]$ in x direction and $[-a, a]$ in y direction. At point B with coordinate $(\varsigma, \zeta, 0)$, the cutting pressure due to P is p_n as the normal component and p_t as the tangential component. The stress at Point $A(x, y, z)$ in the semi-half space is marked as $\{\sigma_x, \sigma_y, \sigma_z, \tau_x, \tau_y, \tau_z\}$ with $|AB| = R$ and the projection of AB to Oxy surface is $|A'B| = r$.

3.2.2 Solution Formulation

The classic problem of an elastic half-space subjected to a point load was solved by Boussinesq (1885) and Cerruti (1882). The solution of stress components for Boussinesq's problem in which a vertical concentrated load is applied on the free surface is shown in (3.1), and the solution of stress components for Cerruti's problem in which a vertical concentrated load is applied is shown in (3.2).

$$
\begin{cases}
\sigma_{xx}^{n} &= \dfrac{3x^2 z}{2\pi R^5} P_n - \dfrac{P_n(1-2\upsilon)}{2\pi}\left[\dfrac{x^2-y^2}{Rr^2\left(R+z\right)} + \dfrac{y^2 z}{R^3 r^2}\right] \\
\sigma_{yy}^{n} &= \dfrac{3y^2 z}{2\pi R^5} P_n - \dfrac{P_n(1-2\upsilon)}{2\pi}\left[\dfrac{y^2-x^2}{Rr^2\left(R+z\right)} + \dfrac{x^2 z}{R^3 r^2}\right] \\
\sigma_{zz}^{n} &= \dfrac{3z^3}{2\pi R^5} P_n \\
\sigma_{yz}^{n} &= \dfrac{3yz^2}{2\pi R^5} P_n \\
\sigma_{xz}^{n} &= \dfrac{3xz^2}{2\pi R^5} P_n \\
\sigma_{xy}^{n} &= \dfrac{3xyz}{2\pi R^5} P_n - \dfrac{P_n(1-2\upsilon)}{2\pi}\left[\left(\dfrac{xy}{Rr^2\left(R+z\right)}\right) - \dfrac{xyz}{R^3 r^2}\right]
\end{cases}
\tag{3.1}
$$

and

$$
\begin{cases}
\sigma_{xx}^{t} &= -\dfrac{3x^3}{2\pi R^5} P_t + \dfrac{x}{2\pi R^3\left(R+z\right)^2}\left(R^2 - y^2 - \dfrac{2Ry^2}{R+z}\right) P_t(1-2\upsilon) \\
\sigma_{yy}^{t} &= -\dfrac{3xy^2}{2\pi R^5} P_t + \dfrac{x}{2\pi R^3\left(R+z\right)^2}\left(3R^2 - x^2 - \dfrac{2Rx^2}{R+z}\right) P_t(1-2\upsilon) \\
\sigma_{zz}^{t} &= -\dfrac{3xz^2}{2\pi R^5} P_t \\
\sigma_{yz}^{t} &= -\dfrac{3xyz}{2\pi R^5} P_t \\
\sigma_{xz}^{t} &= -\dfrac{3x^2 z}{2\pi R^5} P_t \\
\sigma_{xy}^{t} &= -\dfrac{3x^2 y}{2\pi R^5} P_t + \dfrac{x}{2\pi R^3\left(R+z\right)^2}\left(-R^2 + x^2 + \dfrac{2Rx^2}{R+z}\right) P_t(1-2\upsilon)
\end{cases}
\tag{3.2}
$$

The solution to the problem starts from the solutions to these two classic problems. In this problem, the external load is no longer static but dynamic, and the material constants are also time-varying due to the internal damping introduced by viscoelasticity. Under linear viscoelastic assumption, the solutions for viscoelastic half-space subjected to point tangential and normal load could be directly derived by applying the elastic-

viscoelastic correspondence principle (Lakes 1998). The solution (3.1) and (3.2) in viscoelastic cases are then obtained and written as:

$$\begin{cases} \sigma_{xx}^{n} = \dfrac{3x^2 z}{2\pi R^5} P_n - \dfrac{1}{2\pi}\left[\dfrac{x^2 - y^2}{Rr^2\left(R+z\right)} + \dfrac{y^2 z}{R^3 r^2}\right]\displaystyle\int_0^t P_n\left(\tau\right) V\left(t-\tau\right) d\tau \\ \sigma_{yy}^{n} = \dfrac{3y^2 z}{2\pi R^5} P_n - \dfrac{1}{2\pi}\left[\dfrac{y^2 - x^2}{Rr^2\left(R+z\right)} + \dfrac{x^2 z}{R^3 r^2}\right]\displaystyle\int_0^t P_n\left(\tau\right) V\left(t-\tau\right) d\tau \\ \sigma_{zz}^{n} = \dfrac{3z^3}{2\pi R^5} P_n \\ \sigma_{yz}^{n} = \dfrac{3yz^2}{2\pi R^5} P_n \\ \sigma_{xz}^{n} = \dfrac{3xz^2}{2\pi R^5} P_n \\ \sigma_{xy}^{n} = \dfrac{3xyz}{2\pi R^5} P_n - \dfrac{1}{2\pi}\left[\left(\dfrac{xy}{Rr^2\left(R+z\right)}\right) - \dfrac{xyz}{R^3 r^2}\right]\displaystyle\int_0^t P_n\left(\tau\right) V\left(t-\tau\right) d\tau \end{cases} \tag{3.3}$$

and

$$\begin{cases} \sigma_{xx}^{t}\left(x,y,z,t\right) = -\dfrac{3x^3}{2\pi R^5} P_t + \dfrac{x}{2\pi R^3\left(R+z\right)^2}\left(R^2 - y^2 - \dfrac{2Ry^2}{R+z}\right)\displaystyle\int_0^t P_t\left(\tau\right) V\left(t-\tau\right) d\tau \\ \sigma_{yy}^{t}\left(x,y,z,t\right) = -\dfrac{3xy^2}{2\pi R^5} P + \dfrac{x}{2\pi R^3\left(R+z\right)^2}\left(3R^2 - x^2 - \dfrac{2Rx^2}{R+z}\right)\displaystyle\int_0^t P_t\left(\tau\right) V\left(t-\tau\right) d\tau \\ \sigma_{zz}^{t}\ \left(x,y,z,t\right) = -\dfrac{3xz^2}{2\pi R^5} P_t \\ \sigma_{yz}^{t}\left(x,y,z,t\right) = -\dfrac{3xyz}{2\pi R^5} P_t \\ \sigma_{xz}^{t}\left(x,y,z,t\right) = -\dfrac{3x^2 z}{2\pi R^5} P_t \\ \sigma_{xy}^{t}\left(x,y,z,t\right) = -\dfrac{3x^2 y}{2\pi R^5} P_t + \dfrac{x}{2\pi R^3\left(R+z\right)^2}\left(-R^2 + x^2 + \dfrac{2Rx^2}{R+z}\right)\displaystyle\int_0^t P_t\left(\tau\right) V\left(t-\tau\right) d\tau \end{cases} \tag{3.4}$$

Notice that in the above two sets of solutions, all stress components and external forces are functions of spatial variables *x*, *y* and *z* and time *t*. Under the linear viscoelasticity assumption, the ultimate stress field can be calculated as the

superimposition of two independent stress fields: one yielded by tangential distributive forces $P_t(x,y,t)$ and another one by vertical distributive forces $P_n(x,y,t)$. The magnitude of these two forces are determined by the magnitude of the actual external force $P(x,y,t)$ and the slicing angle α. Their relationships are shown as:

$$\begin{cases} P_n(x,y,t) = P(x,y,t)\cos\alpha \\ P_t(x,y,t) = P(x,y,t)\sin\alpha \end{cases}$$

There is also a function V appearing in the solution representing the viscoelasticity of the material, and it is a function of time t. The function $V(t)$ represents the viscoelasticity of the material, and can also be determined by the elastic-viscoelastic correspondence principle (Zhang 1984). The counterpart of V in the elastic solution is $1-2\upsilon$, where υ is the Poisson's ratio. From the relationship between elastic material constants, $1-2\upsilon$ can be expressed as shown in (3.5), where E, G and K denote the Young's modulus, shear modulus and bulk modulus.

$$V = 1-2\upsilon = \frac{3G}{G+3K} = \frac{E}{3K} \tag{3.5}$$

A general way to obtain the expression of $V(t)$ is to apply the elastic-viscoelastic correspondence principle and requires the knowledge of tensile(Young's) relaxation modulus and bulk relaxation modulus. In our study, since the behavior of tensile relaxation is much stronger than the bulk relaxation, the bulk relaxation modulus could be viewed as constant, so that the correspondence principle gives a simple form of $V(t)$ in the Laplace domain as shown in (3.6).

$$\hat{V}(s) = \frac{\hat{E}(s)}{3K} \tag{3.6}$$

Taking inverse Laplace transform, the time-domain expression of $V(t)$ can be obtained by simply changing the Laplace domain terns in both sides of the equation to $V(t)$ and $E(t)$. The result will appear as the convolution terms in (3.3) and (3.4).

With viscoelasticity considered, the second step is to integrate the solution to concentrated force over the arbitrarily defined region *S*, on which the distributed forces are applied. Since the analytic solutions are available, the integration is achieved with the aid of MATLAB using a numerical surface integration function. In this problem, the regions *S* is modeled as a rectangular area in $2a*2b$ (see Figure 3.4). The surface integration is performed using the scheme as shown in Figure 3.4 using two integrating variables ξ and η over the rectangular region *S* ($-a<\xi<a$, $-b<\eta<\beta$). The surface integration is independent of time; therefore, only the coefficients of time-varying terms in solution (3.3) and (3.4) need integrated. Solutions (3.3) and (3.4) are rewritten in (3.7) and (3.8) with some auxiliary functions, in order to simplify the writing for integration later. Notice that, in (3.7) and (3.8), the spatial terms and chronic terms are separated, and this will simplify the following integration.

$$\begin{cases} \sigma_{xx}^{n}(\mathrm{x,y,z,t}) = \dfrac{f_{xx1}(x,y,z)}{2\pi} P_n(t) + \dfrac{f_{xx2}(x,y,z)}{2\pi} P_n(t) * V(t) \\ \sigma_{yy}^{n}(\mathrm{x,y,z,t}) = \dfrac{f_{yy1}(x,y,z)}{2\pi} P_n(t) + \dfrac{f_{yy2}(x,y,z)}{2\pi} P_n(t) * V(t) \\ \sigma_{zz}^{n}(\mathrm{x,y,z,t}) = \dfrac{f_{zz1}(x,y,z)}{2\pi} P_n(t) \\ \sigma_{yz}^{n}(\mathrm{x,y,z,t}) = \dfrac{f_{yz1}(x,y,z)}{2\pi} P_n(t) \\ \sigma_{xz}^{n}(\mathrm{x,y,z,t}) = \dfrac{f_{xz1}(x,y,z)}{2\pi} P_n(t) \\ \sigma_{xy}^{n}(\mathrm{x,y,z,t}) = \dfrac{f_{xy1}(x,y,z)}{2\pi} P_n(t) + \dfrac{f_{xy2}(x,y,z)}{2\pi} P_n(t) * V(t) \end{cases} \tag{3.7}$$

$$
\begin{cases}
\sigma_{xx}^{t}\left(\mathrm{x,y,z,t}\right) &= \dfrac{g_{xx1}\left(x,y,z\right)}{2\pi}P_t\left(t\right)+\dfrac{g_{xx2}\left(x,y,z\right)}{2\pi}P_t\left(t\right)*V\left(t\right)\\
\sigma_{yy}^{t}\left(\mathrm{x,y,z,t}\right) &= \dfrac{g_{yy1}\left(x,y,z\right)}{2\pi}P_t\left(t\right)+\dfrac{g_{yy2}\left(x,y,z\right)}{2\pi}P_t\left(t\right)*V\left(t\right)\\
\sigma_{zz}^{t}\left(\mathrm{x,y,z,t}\right) &= \dfrac{g_{zz1}\left(x,y,z\right)}{2\pi}P_t\left(t\right)\\
\sigma_{yz}^{t}\left(\mathrm{x,y,z,t}\right) &= \dfrac{g_{yz1}\left(x,y,z\right)}{2\pi}P_t\left(t\right)\\
\sigma_{xz}^{t}\left(\mathrm{x,y,z,t}\right) &= \dfrac{g_{xz1}\left(x,y,z\right)}{2\pi}P_t\left(t\right)\\
\sigma_{xy}^{t}\left(\mathrm{x,y,z,t}\right) &= \dfrac{g_{xy1}\left(x,y,z\right)}{2\pi}P_t\left(t\right)+\dfrac{g_{xy2}\left(x,y,z\right)}{2\pi}P_t\left(t\right)*V\left(t\right)
\end{cases}
\tag{3.8}
$$

The surface integration follows the expressions as shown in (3.9) and (3.10):

$$
\begin{cases}
\sigma_{xx}^{n}\left(\mathrm{x,y,z,t}\right)=P_n\left(t\right)\iint\limits_S\dfrac{f_{xx1}\left(\xi-x,\eta-y,z\right)}{2\pi}d\xi d\eta+P_n\left(t\right)*V\left(t\right)\iint\limits_S\dfrac{f_{xx2}\left(\xi-x,\eta-y,z\right)}{2\pi}d\xi d\eta\\
\sigma_{yy}^{n}\left(\mathrm{x,y,z,t}\right)=P_n\left(t\right)\iint\limits_S\dfrac{f_{yy1}\left(\xi-x,\eta-y,z\right)}{2\pi}d\xi d\eta+P_n\left(t\right)*V\left(t\right)\iint\limits_S\dfrac{f_{yy2}\left(\xi-x,\eta-y,z\right)}{2\pi}d\xi d\eta\\
\sigma_{zz}^{n}\left(\mathrm{x,y,z,t}\right)=P_n\left(t\right)\iint\limits_S\dfrac{f_{zz1}\left(\xi-x,\eta-y,z\right)}{2\pi}d\xi d\eta\\
\sigma_{yz}^{n}\left(\mathrm{x,y,z,t}\right)=P_n\left(t\right)\iint\limits_S\dfrac{f_{yz1}\left(\xi-x,\eta-y,z\right)}{2\pi}d\xi d\eta\\
\sigma_{xz}^{n}\left(\mathrm{x,y,z,t}\right)=P_n\left(t\right)\iint\limits_S\dfrac{f_{xz1}\left(\xi-x,\eta-y,z\right)}{2\pi}d\xi d\eta\\
\sigma_{xy}^{n}\left(\mathrm{x,y,z,t}\right)=P_n\left(t\right)\iint\limits_S\dfrac{f_{xy1}\left(\xi-x,\eta-y,z\right)}{2\pi}d\xi d\eta+P_n\left(t\right)*V\left(t\right)\iint\limits_S\dfrac{f_{xy2}\left(\xi-x,\eta-y,z\right)}{2\pi}d\xi d\eta
\end{cases}
\tag{3.9}
$$

$$
\begin{cases}
\sigma_{xx}^{t}\left(\mathrm{x,y,z,t}\right)=P_t\left(t\right)\iint\limits_S\dfrac{g_{xx1}\left(\xi-x,\eta-y,z\right)}{2\pi}d\xi d\eta+P_t\left(t\right)*V\left(t\right)\iint\limits_S\dfrac{g_{xx2}\left(\xi-x,\eta-y,z\right)}{2\pi}d\xi d\eta\\
\sigma_{yy}^{t}\left(\mathrm{x,y,z,t}\right)=P_t\left(t\right)\iint\limits_S\dfrac{g_{yy1}\left(\xi-x,\eta-y,z\right)}{2\pi}d\xi d\eta+P_t\left(t\right)*V\left(t\right)\iint\limits_S\dfrac{g_{yy2}\left(\xi-x,\eta-y,z\right)}{2\pi}d\xi d\eta\\
\sigma_{zz}^{t}\left(\mathrm{x,y,z,t}\right)=P_t\left(t\right)\iint\limits_S\dfrac{g_{zz1}\left(\xi-x,\eta-y,z\right)}{2\pi}d\xi d\eta\\
\sigma_{yz}^{t}\left(\mathrm{x,y,z,t}\right)=P_t\left(t\right)\iint\limits_S\dfrac{g_{yz1}\left(\xi-x,\eta-y,z\right)}{2\pi}d\xi d\eta\\
\sigma_{xz}^{t}\left(\mathrm{x,y,z,t}\right)=P_t\left(t\right)\iint\limits_S\dfrac{g_{xz1}\left(\xi-x,\eta-y,z\right)}{2\pi}d\xi d\eta\\
\sigma_{xy}^{t}\left(\mathrm{x,y,z,t}\right)=P_t\left(t\right)\iint\limits_S\dfrac{g_{xy1}\left(\xi-x,\eta-y,z\right)}{2\pi}d\xi d\eta+P_t\left(t\right)*V\left(t\right)\iint\limits_S\dfrac{g_{xy2}\left(\xi-x,\eta-y,z\right)}{2\pi}d\xi d\eta
\end{cases}
\tag{3.10}
$$

Notice that the stress components are redefined after the surface integration, and also, r and R are defined as:

$$r^2 = (\xi - x)^2 + (\eta - y)^2$$
$$R^2 = (\xi - x)^2 + (\eta - y)^2 + z^2$$

Due to the complexity of perform analytical integration, during the actual calculation of all these stress components, numerical integrations were used instead. The numerical integrations were achieved using the MATLAB function "*quad2d"*, which numerically evaluate double integral using tiled method. *q = quad2d(fun,a,b,c,d)* approximates the integral of "*fun(x,y)*" over the planar region $a \leqslant x \leqslant b$ and $c(x) \leqslant y \leqslant d(x)$. "*fun"* is a function handle, *c* and *d* may each be a scalar or a function handle.

Among all expressions of stress components, the surface integration of the stress components f_{xx2}, f_{yy2} and f_{xy2}, for vertical load have singularities at points where $r = 0$. These singularities could be smoothed because they actually converge at those points. However, the MATLAB integration pattern doesn't recognize this situation and will report an error if the point of interest has the coordinates with $r = 0$.

To avoid such a problem, the integration for these three stress components was performed with a special scheme, as shown in Figure 3.5. A very small parameter ε was used to avoid the integration variables ξ and η from moving to point (*x, y*), which makes $r = 0$. With ε, the original integration region *S* was divided into five sub-regions. The smallest region contains the singularity point. According to the Mean value theorem of integrals and limit theory, when ε is small enough, the integral over this small square will converge to zero. With a very small ε value used, equation (3.11) was assumed to hold:

$$\iint_S (\ )d\eta d\xi = \iint_{\text{Region 1}} (\ )d\eta d\xi + \iint_{\text{Region 2}} (\ )d\eta d\xi + \iint_{\text{Region 3}} (\ )d\eta d\xi + \iint_{\text{Region 4}} (\ )d\eta d\xi \qquad (3.11)$$

The MATLAB function *quad2d* also provides a method to control the error so that the result will be controlled in a reasonable range.

During implementation, each stress component for both vertical and tangential distributed loads was defined as a *m-file* in MATLAB, and with the point of interest given, the stress could then be calculated.

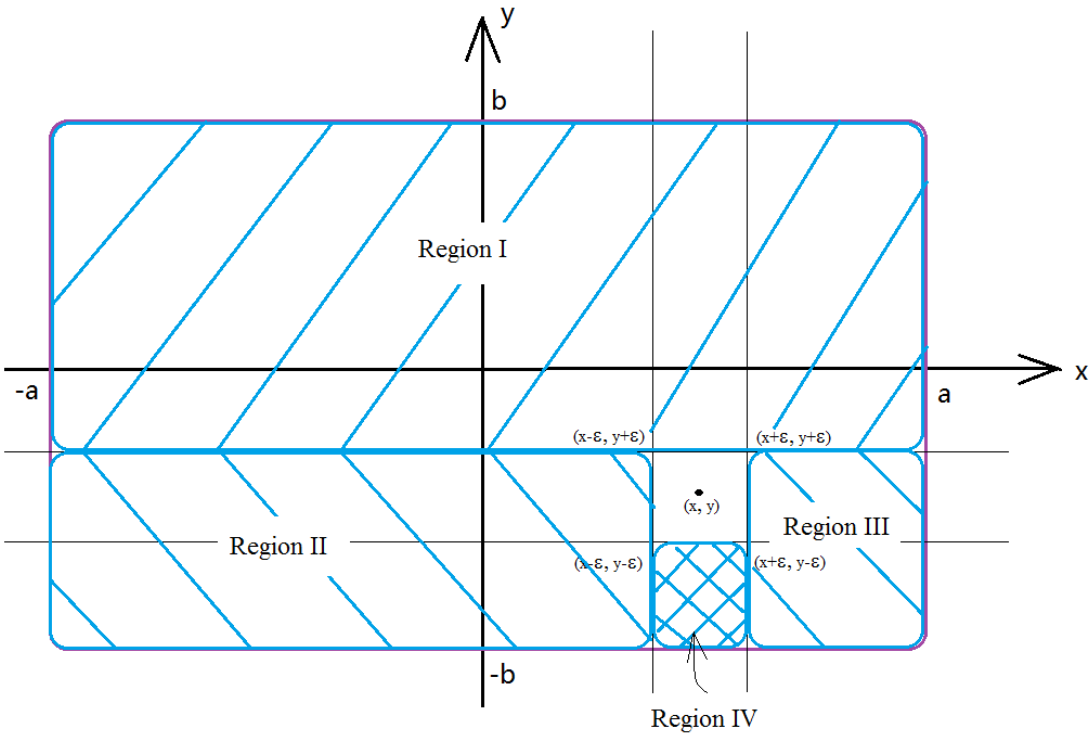

Figure 3.5 Numerical integration over region S by four divisions

The above mentioned integration scheme only works for the spatial terms. As for the time-varying viscoelastic convolution, another MATLAB function "*conv*" was used. *w = conv(u,v)* convolves vectors *u* and *v*. Algebraically, convolution is the same operation as multiplying the polynomials whose coefficients are the elements of *u* and *v*. In this research, there are convolutions between the external loads and the viscoelastic relaxation

modulus. The external load condition was subjectively assigned so that the function was fixed. The relaxation modulus could be determined experimentally. In this study, some arbitrarily defined values were used.

The MATLAB codes for this chapter are enclosed in the Appendix of this dissertation.

3.2.3 Failure Analysis

The computational models developed in injury biomechanics aim at predicting physiological mechanical behavior as well as the damage and failure of biological tissues. The challenge (Subit , Chabrand and Masson 2009) is to link the concept of 'lesion' used in clinical diagnostics, to the concepts of 'damage' and 'failure' used in mechanical modeling and system analysis. The lesions reported in clinical studies are obviously linked to the structure of the injured organ at various levels, and their severity is associated to the type of mechanical damage the organ sustains. Computational models are developed to assess tissues failure from mechanical parameters determined based upon experimental tests and the choice of a mechanical model.

In this study, the mechanical behavior of the soft biological tissues is evaluated, which are modeled as the linear, isotropic, homogenous viscoelastic half-space. Through the stress field calculation and by applying failure criteria, it's expected to link the mechanical behavior of the soft tissues with the clinical observation and provide means to improve diagnosis and treatment of soft tissue injuries. Attention is paid to the understanding of patterns of stress field and the effects of viscoelasticity on the stress distribution.

Material failure refers to the complete loss of load carrying capacity that results from progressive degradation of the material stiffness. Stiffness degradation is modeled using damage mechanics. In this study, the Tresca criterion of material failure, also known as maximal shear stress, raised by the French Mechanical engineer Henri Édouard Tresca, was introduced. The criterion specifies that a material would flow plastically if

$$\sigma_{Tresca} > \sigma_1 - \sigma_3 > \sigma_{Max} \tag{3.12}$$

In (3.12), σ_1 and σ_3 are the maximum and minimum principal stresses, which can be calculated by choosing a particular coordinate system for the original stress tensor so that the shear stresses vanish. The corresponding matrix for coordinates transformation can be constructed by using the eigenvectors of the stress tensor. The maximum shear stress, or the Tresca stress, is calculated as the difference between the maximum and minimum principal stresses. The Tresca criterion states that the material will yield if the Tresca stress exceeds the maximum allowable value.

In this study, since the value of stress components are all stored in MATLAB variables, the MATLAB function "*eig*" could be used to achieve such a purpose. As described in MATLAB documents, **d** = *eig(***A***)* returns a vector of the eigenvalues of matrix **A** and **d** = *eig*(**A**, **B**) returns a vector containing the generalized eigenvalues, if **A** and **B** are square matrices. The eigenvalues are the corresponding three principal stresses.

3.3 Stage II Modeling: FEM Simulation of Continuous Cutting

The contact problem discussed in the previous section could be viewed as an initial step of a whole cutting process. The stress field information provides a good insight of the effects of the blade on the body. Failures could be predicted based on the

obtained information. The analytic solutions provide a convenient way to obtain these results. Even though a numerical superimposition scheme was introduced, the computation complexity is much lower than a FEM-based numerical method. However, after the body material's rupture, the proceeding of the hard object will lead to cutting. The cutting process involves large deformation and complex geometry, both of which make it very difficult to obtain the analytic form of solutions. To deal with such problems, the finite element method (FEM) is a good choice.

FEM has been fast developed during the last century. With renovations of CPUs, computers are now more and more capable of handling FEM problems with a large number of elements. In this study, FEM software was used to simulate the cutting process after the rupture. ABAQUS was used to establish the cutting model, mesh the model and run the simulation.

In this study, particular interest is given to the cutting process of a bi-layered object. The upper layer is comprised of soft viscoelastic material, and the lower layer is comprised of hard material. Such a model has many applications, such as a cement-soil model, or a bone-tissue model. Taking the bone-tissue model as an example, the material of the upper layer is soft biological tissue, which was modeled as isotopic and homogenous linear viscoelastic material. The viscoelasticity was obtained from the tensile relaxation tests, as introduced in Chapter 4. The lower layer which represents the bones was modeled as isotopic and homogeneous linear elastic material with a comparatively high Young's modulus ($E = 1Gpa$). The purpose is to obtain the force response on the blade during the whole cutting process, especially when the blade approaches the interface between the soft tissues and bone. It is expected to find certain

patterns of the blade force, and thus use it to prevent the blade cutting into the bone. This is an application in the food processing industry. Food processing companies suffer from a lot of losses due to the damage of debone blades due to cutting into bones. It is expected to develop such an algorithm to precisely control the blades' motions and reduce the losses.

3.3.1 ABAQUS Solver

ABAQUS is an excellent FEM package developed by ABAQUS, Inc. It provides a complete solver for users to carry out simulations for problems in mechanical engineering and thermal studies. It contains the parts from geometry building, material property defining, assembling, simulating and post-processing. For the problem concerned in this study, the material could be modeled using the viscoelastic property which is available under the elastic properties' category.

Prony series is used for interpreting the viscoelastic effects, with three entries for each Prony series element. The shear relaxation modulus should be specified by assigning the normalized parameters g_k.

During the experiment, the volume relaxation is hardly to be noticed; therefore the volume is assumed not to change during relaxation, so the normalized bulk relaxation function should be held as a constant of 1. For the exponential decaying model, two parameters should be specified.

The volumetric relaxation function for a general Prony series is written as:

$$K_R(t) = K_0\left(1 - \sum_{k=1}^{N} k_k\left(1 - e^{-t/\tau_k}\right)\right).$$

where K_0 is the instantaneous bulk modulus, τ_k is the relaxation time and k_k is the normalized weight of the relaxation to K_0 associated with relaxation time τ_k.

The relaxation for the one order exponential decaying function is:

$$k(t) = \frac{K_R(t)}{K_0} = (1 - k_1) + k_1 e^{-t/\tau_1}.$$

Simply let $k_1 = 0$, then a zero-relaxation of volume could be obtained.

Since the cutting problem is concerned, the shear failure criterion is introduced to eliminate the failed elements from the model.

3.3.2 2D Modeling

When there is only normal cutting force, due to symmetry, a 2D cutting problem is considered. The model is shown in Figure 3.6.

The model consists of two parts, with the upper part representing the soft tissues and the lower part representing bones. Each part is a rectangle solid in the dimension of 15mm by 5mm. Notice that each part is divided into three segments along the X direction. The reason for doing so is to simplify the mesh generation. Since interest is mainly in the cutting part (the middle part), there is no need to spend many meshes on the side parts. Therefore, the meshes are much denser in the middle than in the two sides. The mesh for the whole body is shown in Figure 3.7. Figure 3.8 provides a closer look to meshes on the interface.

The force between the blade and the body was set as an output so that the computer will record the force history for later analysis.

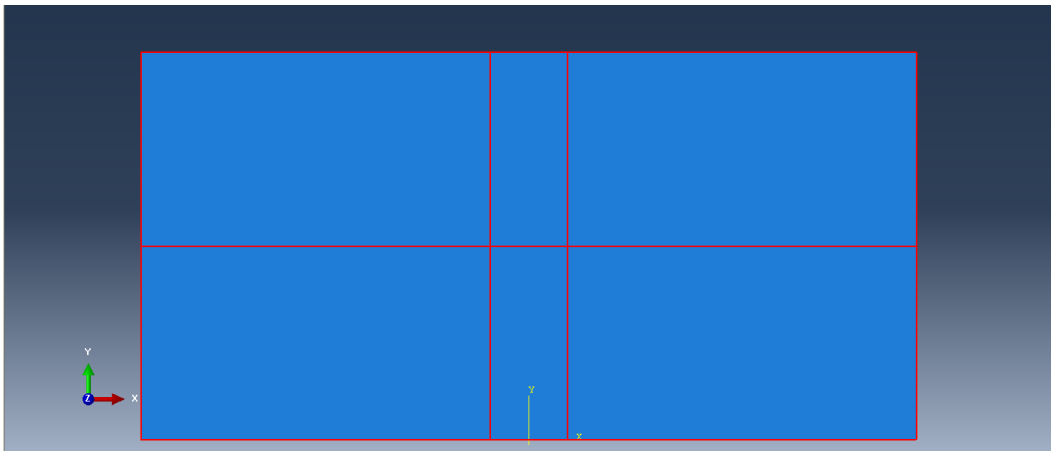

Figure 3.6 Geometry of the 2D cutting model.

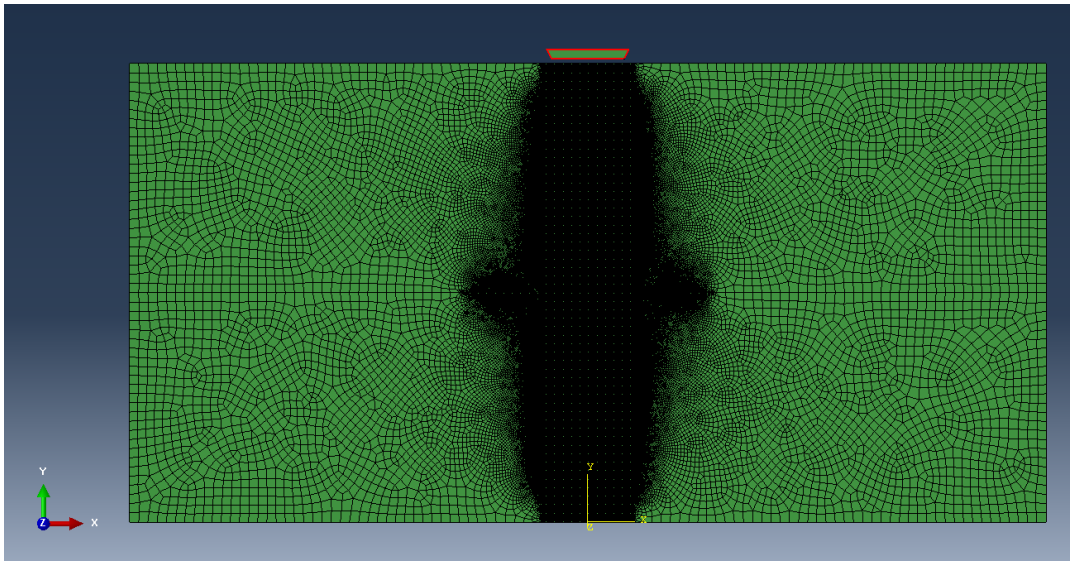

Figure 3.7 Mesh Generation of the 2D model.

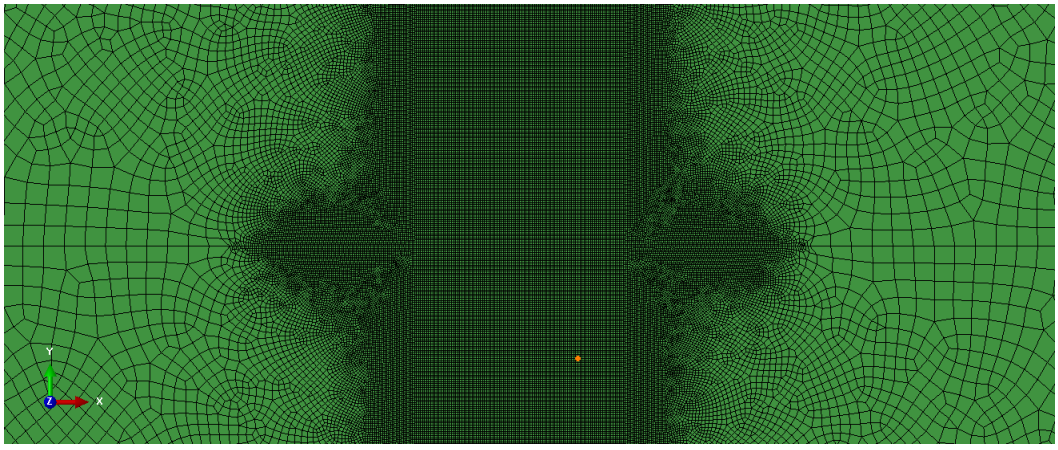

Figure 3.8 Mesh of the 2D cutting modeling near the interface.

3.3.3 3D Modeling

In the 3D model, the blade could move in two directions: negative *x* and negative *z*. The motion in negative *x* corresponds to the slicing motion, and the motion in negative *z* corresponds to the compression cutting in normal direction. The cutting angles are determined by setting different ratios for velocity components of the blade in these two directions. Since the blade is much harder than the bio-materials, it is modeled as a rigid body, which means no deformation at all. The mesh for this body could be very simple as shown in Figure 3.9.

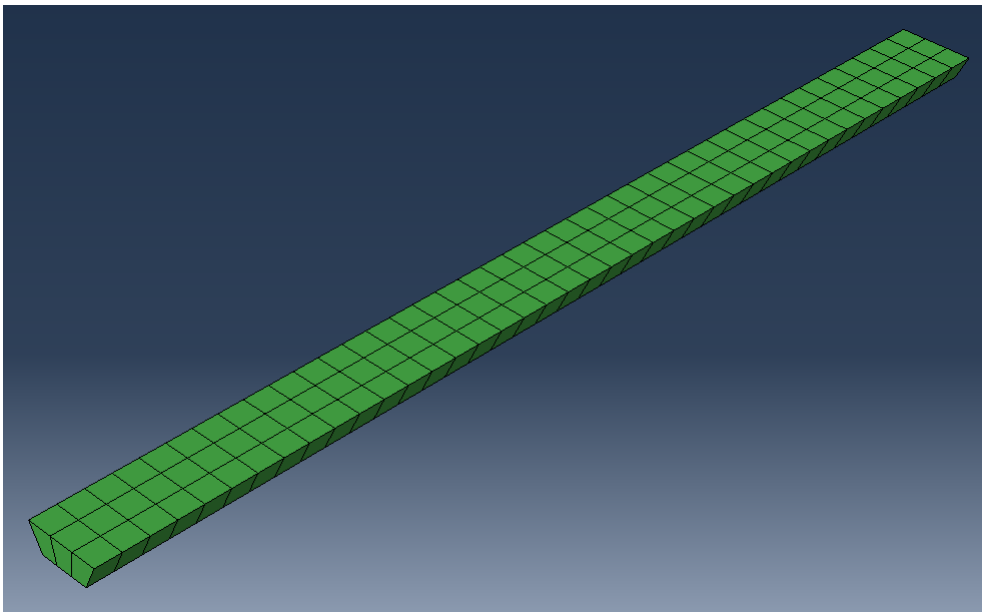

Figure 3.9 Mesh of the blade in 3d cutting model.

The body in the 3D model is also comprised of two layers: the upper layer represents the soft tissues and the lower layer represents the bone tissues. The 3D geometry introduces more complexity than the 2D model because the nodes number is greatly increased. Similarly, seeds are assigned for mesh generation according to the purpose of this study. Seeds in the middle part are much denser than in the two sides. This ensures the results are more reliable. Notice that, only the cutting process when the

blade is in the soft tissue and approaches the interface is the focus, so the bone tissues are meshed in a relatively loose pattern, as shown in Figure 3.10. The whole assembly is shown in Figure 3.11. Notice that the blade length in *x* direction is twice the length of the body in order to make sure that the blade will have full contact with the body during the whole cutting process.

Contact forces, strain energy and fracture work are all set as outputs and are thus available for analysis.

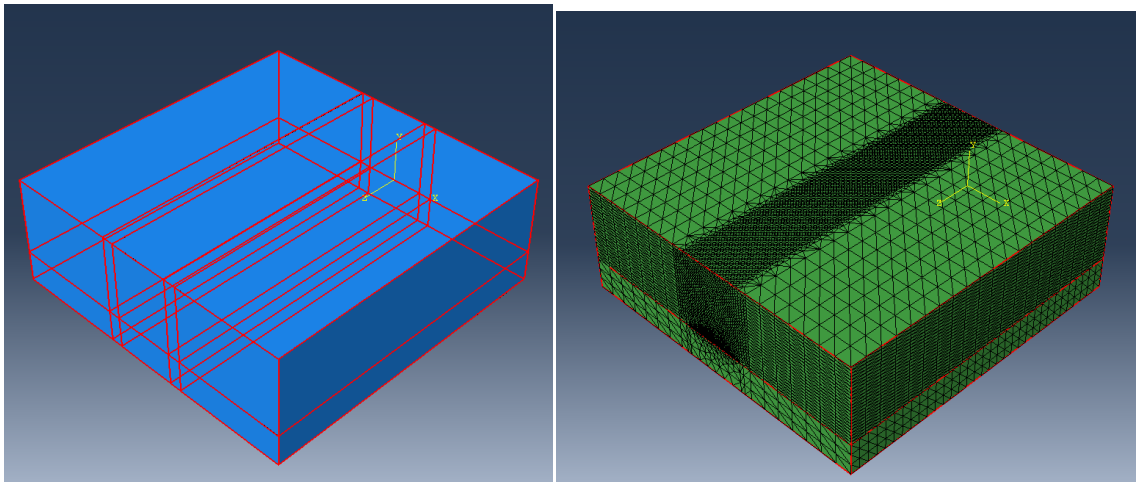

a) Geometry of 3D Model, *b) Mesh of 3D Model,*

Figure 3.10 3D cutting model.

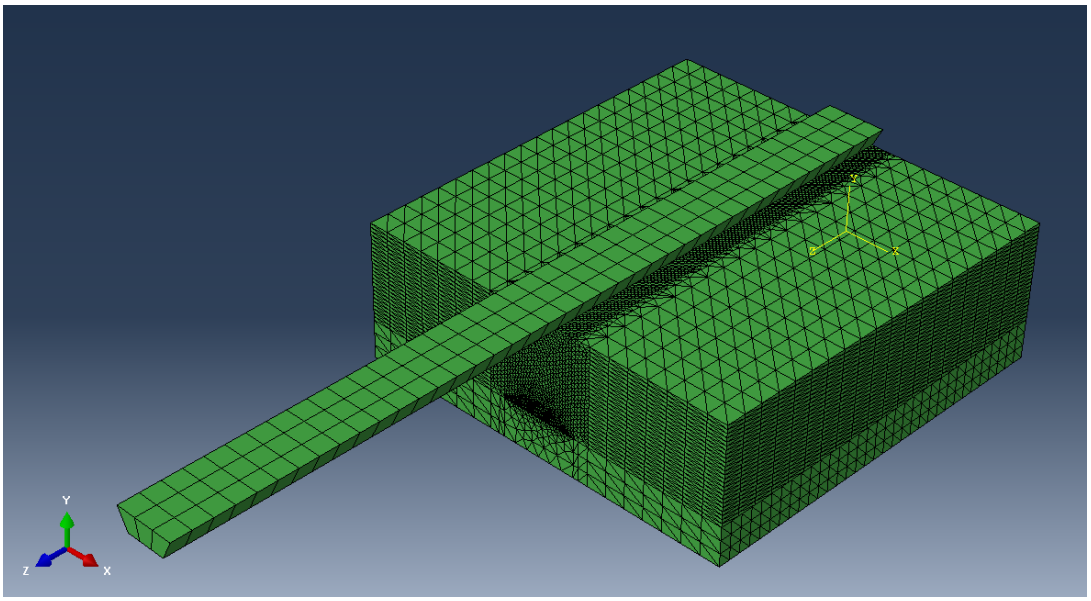

Figure 3.11 Meshed parts assembly of the 3d cutting model.

3.3.4 Solver Setup

The successful running of ABAQUS requires correct parameter settings. Among all those settings, the material properties and boundary conditions are the most important, so they are explained in detail in this section.

Material Properties

The blade is modeled as a hard object with Young's Modulus of 9GPa and a Passion's ratio of 0.3 (see Figure 3.12).

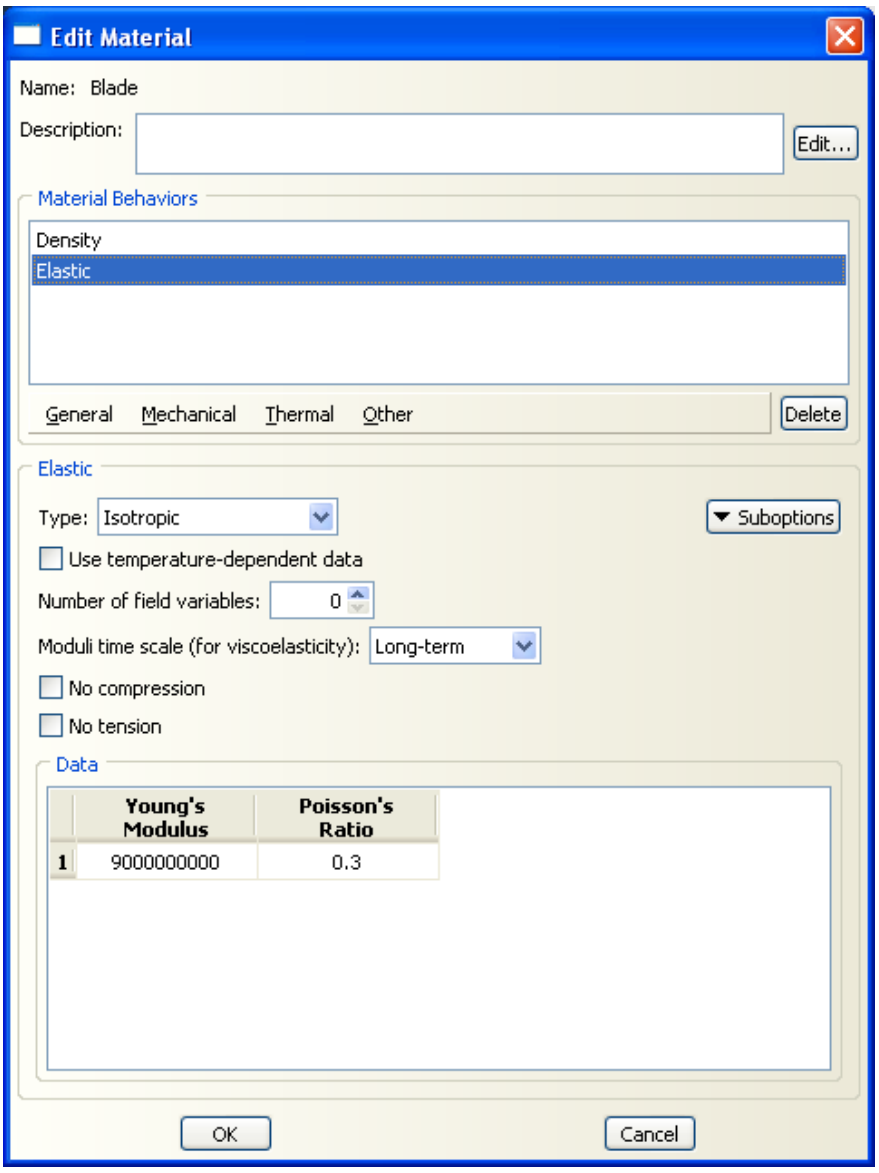

Figure 3.12 Material property setting for the blade.

The bone tissues are modeled as linear homogenous isotropic elastic-plastic material. The data are obtained from previous research. A shear failure criterion is applied for this material (not shown in the editor board). The Young's Modulus is set to 250KPa and the Poisson's ratios is set to 0.4 (see Figure 3.13).

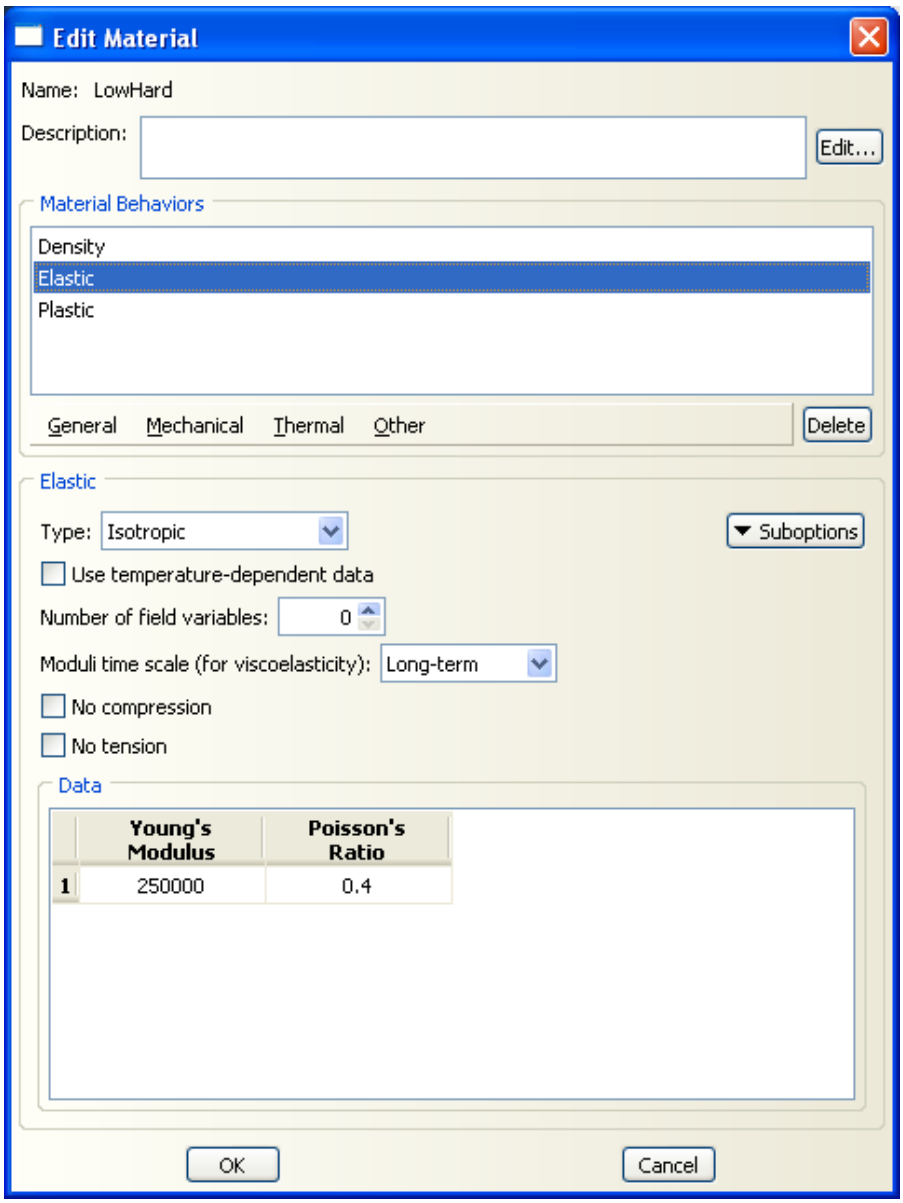

Figure 3.13 Material property settings for bone tissues.

Soft Tissues

The soft tissues are modeled as linear, homogenous, isotropic viscoelastic-plastic material. The data are from the relaxation experiments. The Young's Modulus is set to 12.5KPa and the Poisson's ratio is set to 0.45, which is very close to an incompressible material. A shear failure criterion is also applied to this material so that element deletion will be performed for failed elements. The settings are shown in Figure 3.14.

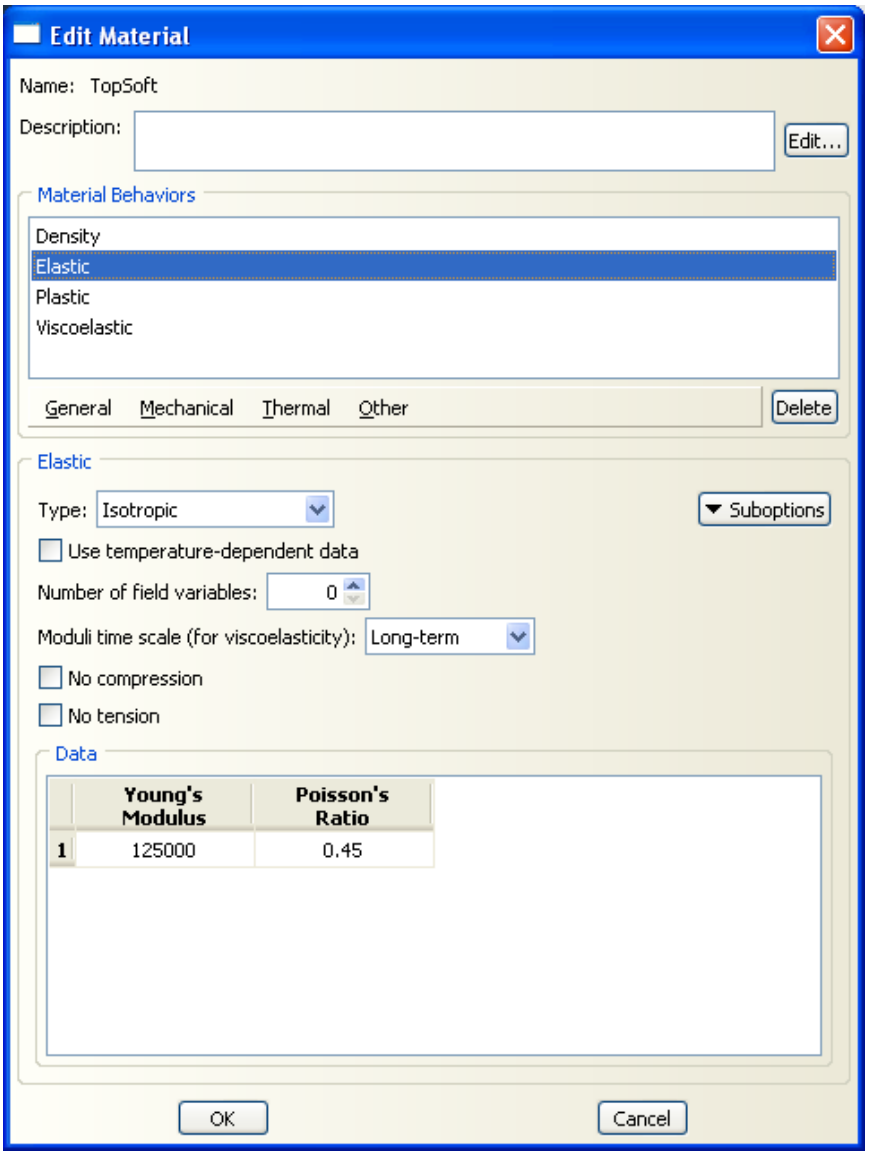

Figure 3.14 Material property settings for soft tissues.

Interaction Modeling

The interaction between the blade and the biomaterial body is described in the interaction interface (see Figure 3.15). The contact type is set as surface to surface contact, and the mechanical constraint formulation is set to Kinematic contact method. The part highlighted in red is the first surface of the contact couple, and the part highlighted in purple is the second surface. The prescribed interaction model will

describe the mechanical property (such as the stresses) and kinematic consistence (displacements) between the surfaces and thus make it reasonable.

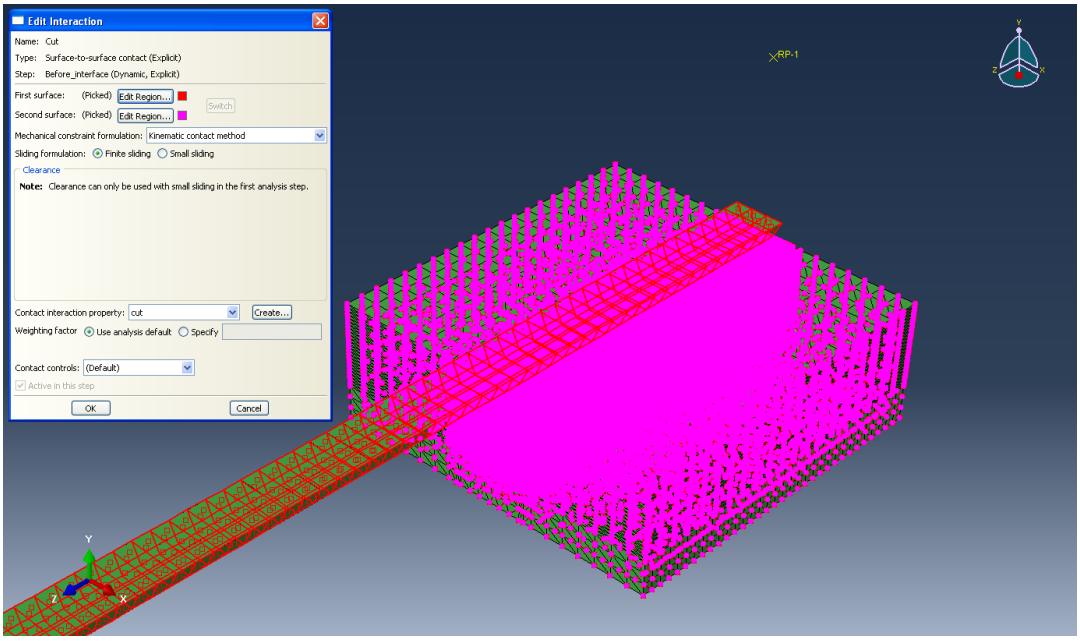

Figure 3.15 Interaction settings for the contact between blade and body.

Boundary Conditions

Boundary conditions are also essential parts for the simulation. A fixed bottom constraint was set to the bottom surface of the body so that it won't run away under slicing forces. In fact, the constraints are applied to all nodes on the bottom surface (see Figure 3.16).

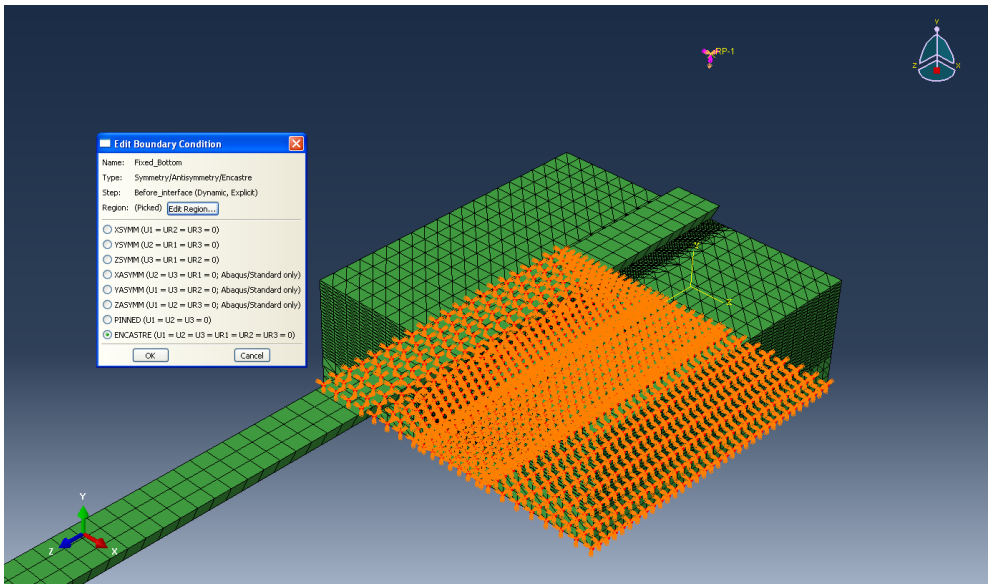

Figure 3.16 Boundary condition setting for the fixed bottom.

A velocity profile is assigned to the blade as shown in Figure 3.17. The reference point is necessary because the blade is described as a rigid body, the velocity of which must be accomplished using a reference point as required by the solver. V1, V2 and V3 are the translational velocities and the other three are rotational velocities. To model the slicing process, only velocities in V1(x) and V3(z) are needed.

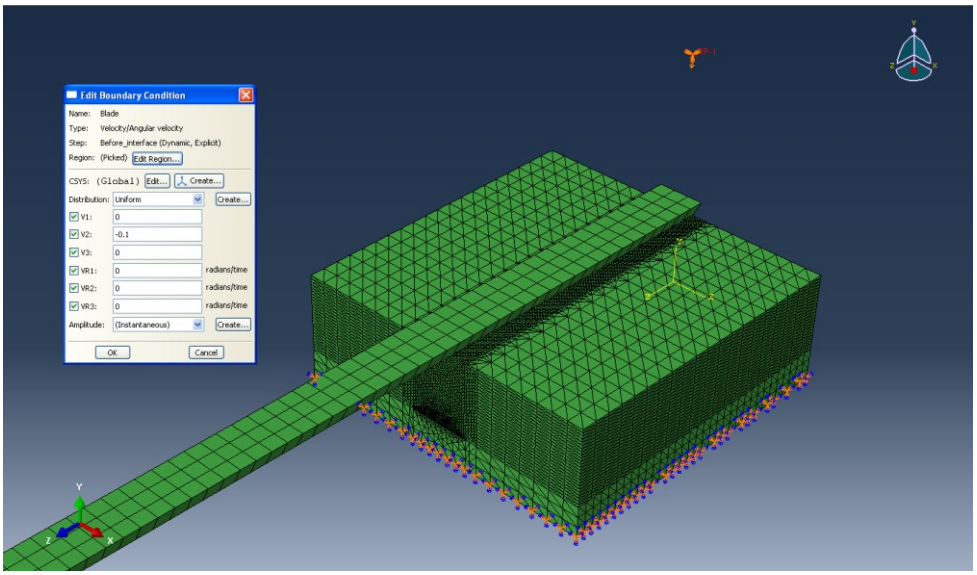

Figure 3.17 Boundary Condition Setting for the Blade Motion

CHAPTER IV EXPERIMENTAL MODELING

As discussed in Chapter 3, the viscoelastic material properties are fundamentally needed in either theoretical calculations or FEM simulations. Those properties could be tensile, shear or bulk moduli. This chapter presents an experimental method to obtain these material properties as parameters used in Chapter 3.

There are many material constants to describe the material's mechanical properties. For an isotropic and homogenous elastic material, these constants could be bulk modulus (*K)*, Young's modulus (*E*), shear modulus (*G*), Poisson's ratio (υ), etc. However, among these material constants, only two are independent. Table 4.1 gives the relationships among these constants. The choice of two parameters could be any combination in the table.

Table 4.1 *Elastic material constants*

	(K, E)	*(K,G)*	*(K, v)*	*(E, G)*	*(E, v)*	*(G, v)*
K				$\frac{\mathrm{EG}}{3(3\mathrm{G}-\mathrm{E})}$	$\frac{\mathrm{EG}}{3(3\mathrm{G}-\mathrm{E})}$	$\frac{\mathrm{EG}}{3(3\mathrm{G}-\mathrm{E})}$
E		$\frac{9\mathrm{KG}}{3\mathrm{K}+\mathrm{G}}$	$3K(1-2v)$			$2G(1+v)$
G	$\frac{3\mathrm{KE}}{9\mathrm{K}-\mathrm{E}}$		$\frac{3\mathrm{K}(1-2)}{2(1+\mathrm{v})}$		$\frac{\mathrm{E}}{2(1+\mathrm{v})}$	
v	$\frac{3\mathrm{K}-\mathrm{E}}{6\mathrm{K}}$	$\frac{3\mathrm{K}-2\mathrm{G}}{2(3\mathrm{K}+\mathrm{G})}$		$\frac{\mathrm{E}}{2\mathrm{G}}-1$		

4.1 Viscoelastic Material Modulus

The relationships between these four parameters for linear isotopic and homogenous viscoelastic materials are the same as elastic materials. The only difference is that these four parameters are time-dependent. Determination of these material constants could be easy for some certain materials, such as metal or wood. However, for viscoelastic materials, the task is much more difficult: performing two tests on viscoelastic materials is costly and complex. Previous researchers studying the experiment methods have already provided a thorough method to experimentally determine these material properties (Kim, Lee and Kim, 2011). In this study, two assumptions are made to simplify this method: 1) Homogenous and isotropic materials and 2) Poisson's ratio is a time-independent constant. The first assumption has its own limitations, but is still reasonable and acceptable for many engineering materials. The second assumption is based on a quasi-isochoric motion, which is also acceptable to most biomaterials. With these two assumptions, it is only needed to determine one time-dependent material constant, and then we are able to obtain all the other material constants by extending the relationships as shown in Table 4.1 to a viscoelastic background. Note that, the Poisson's ratio being constant greatly simplifies the calculation.

The simplest test is the uniaxial tensile method, which determines the tensile modulus $E(t)$. In this study, tensile relaxation tests were performed on ligaments dissected from chicken wings, and the data was then used in calculations as discussed in Chapter 3 to get the results in Chapter V.

4.2 Specimen Preparations

Eight chickens were bought from local grocery stores. Each one provided two ligaments from wings and another two from legs. Therefore, 16 pairs of ligaments were obtained. The strips were approximately 5mm wide and 10mm long in longitudinal direction. The thickness was about 2-3mm. All dimensions were determined using a caliper.

4.3 Equipment Setup

Illustration for the experiment setup is shown in Figure 4.1 and the equipment used is listed in Table 4.2.

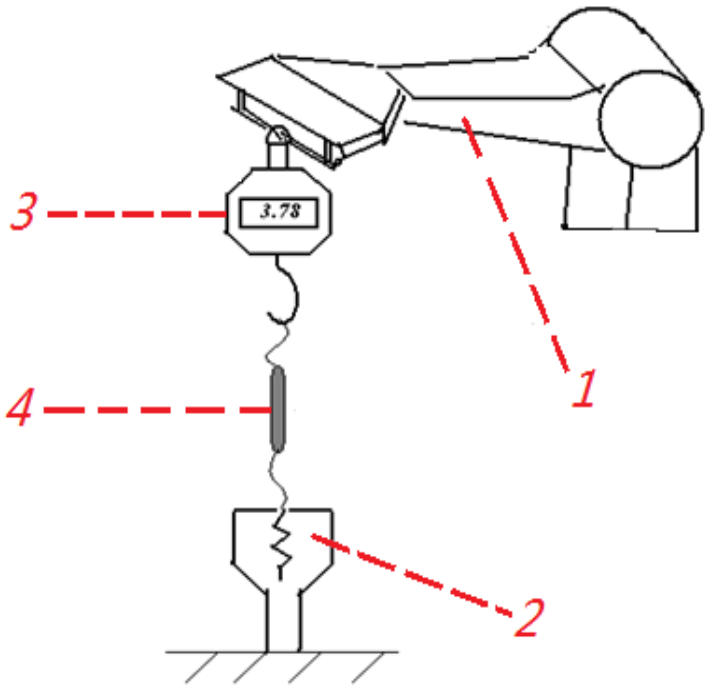

Figure 4.1 Illustration of experimental setup for relaxation test.

Table 4.2 List of equipment

Number	Equipment	Function
1	Computer controlled 6-DOF EPSON robot	Control the motion for stress relaxation
2	Grippers	Hold the ligament firmly
3	Force sensor	Record the relaxation force (N)
4	Camera	Record the relaxation process

Two persons were needed to perform the tests. One was responsible for coding and controlling the computer which manipulates the motion of the robotic hand, and the other was responsible for monitoring the reading and the ligament moisture by spraying water onto it. A photo of actual experiment scene was shown in Figure 4.2, Figure 4.3 and Figure 4.4.

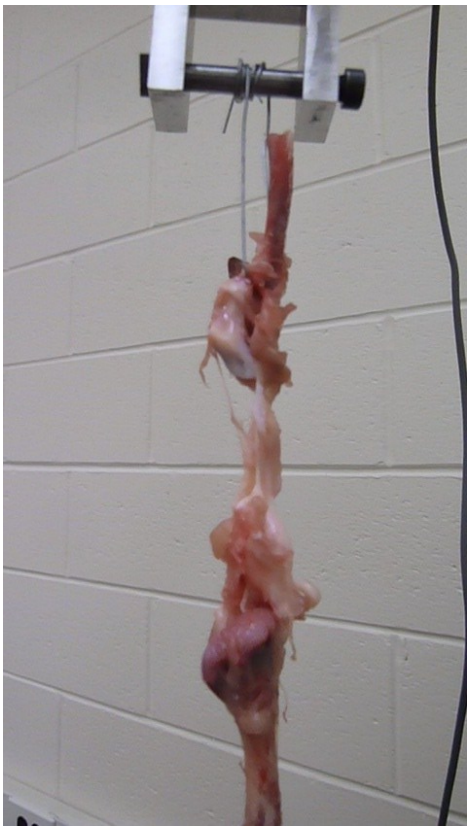

Figure 4.2 Ligament fixation using grippers.

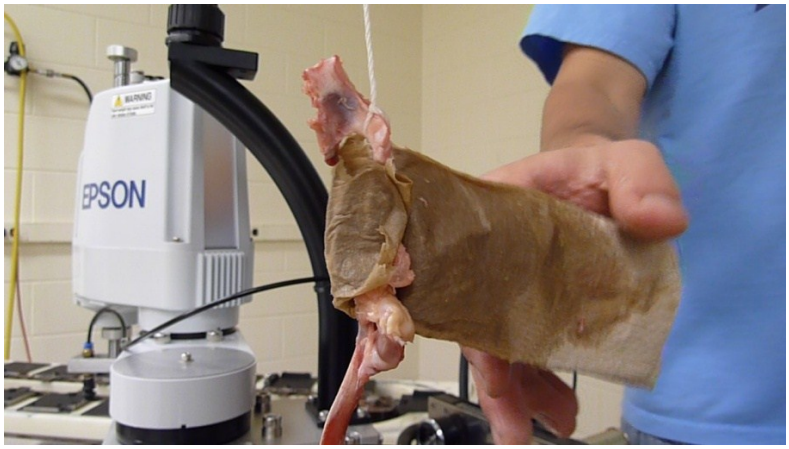

Figure 4.3 Treatment for constant moisture.

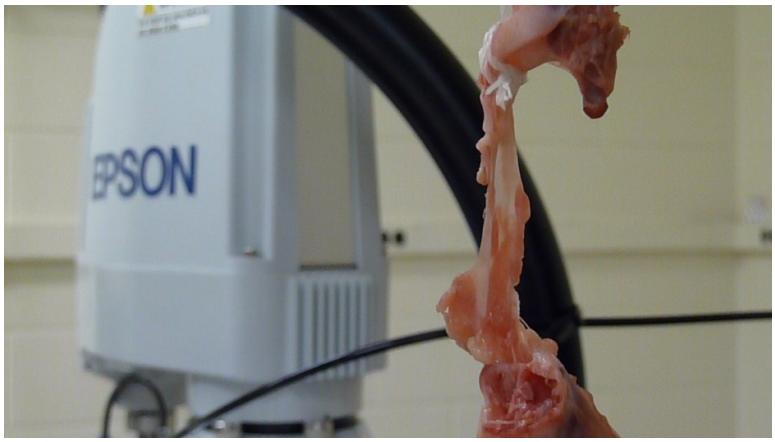

Figure 4.4 Ligament in tensile.

Before relaxation test, all specimens were pre-treated by stretching to a ratio of 1.2 slowly in a speed of 2mm/s for two times. After pretreatment, the relaxation tests were performed with stretch ratio to 1.8. The engineering stresses were determined for the tension. The collected data were used to generate the tensile relaxation function $E(t)$.

4.4 Data Fitting

In this study, the exponential decay function was used for the relaxation function $E(t)$. The experimental data were fitted to the exponential function by the use of MATLAB function "*nlinfit*". The least square method was performed to find the best parameters for the exponential function. The results were organized in Chapter 5.

CHAPTER V CUTTING SIMULATION RESULTS

This chapter presents the analysis of the data obtained from the chicken ligament tension experiments, and the discussion on the numerical results computed using the analytic solutions for the contact problem and the FEM results simulated using the ABAQUS package for the continuous cutting problem.

5.1 Experimental Estimation of Viscoelastic Properties

Among all the relaxation tests, there were several successful groups of data. Three of them are presented in 0, Figure 6.2 and Figure 6.3, respectively.

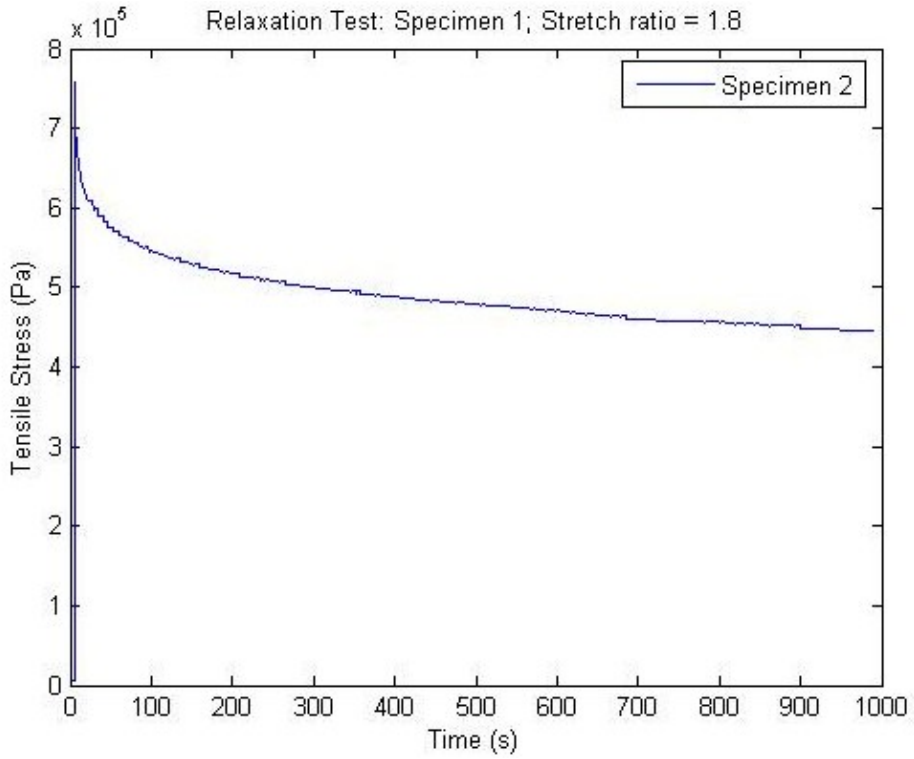

Figure 6.1 Relaxation test for specimen 1.

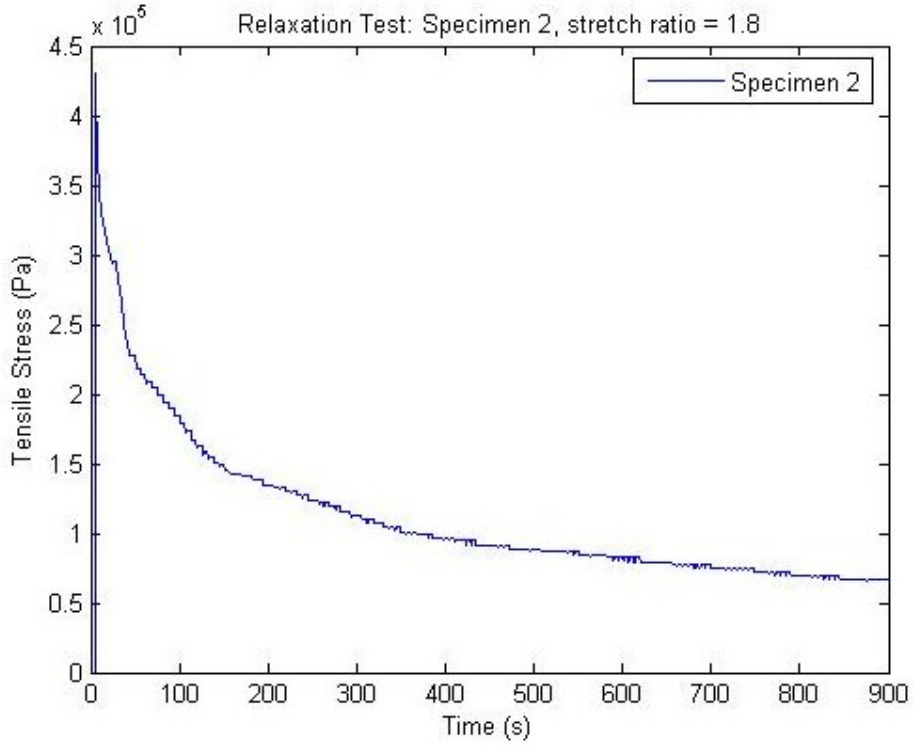

Figure 6.2 Relaxation test for specimen 2.

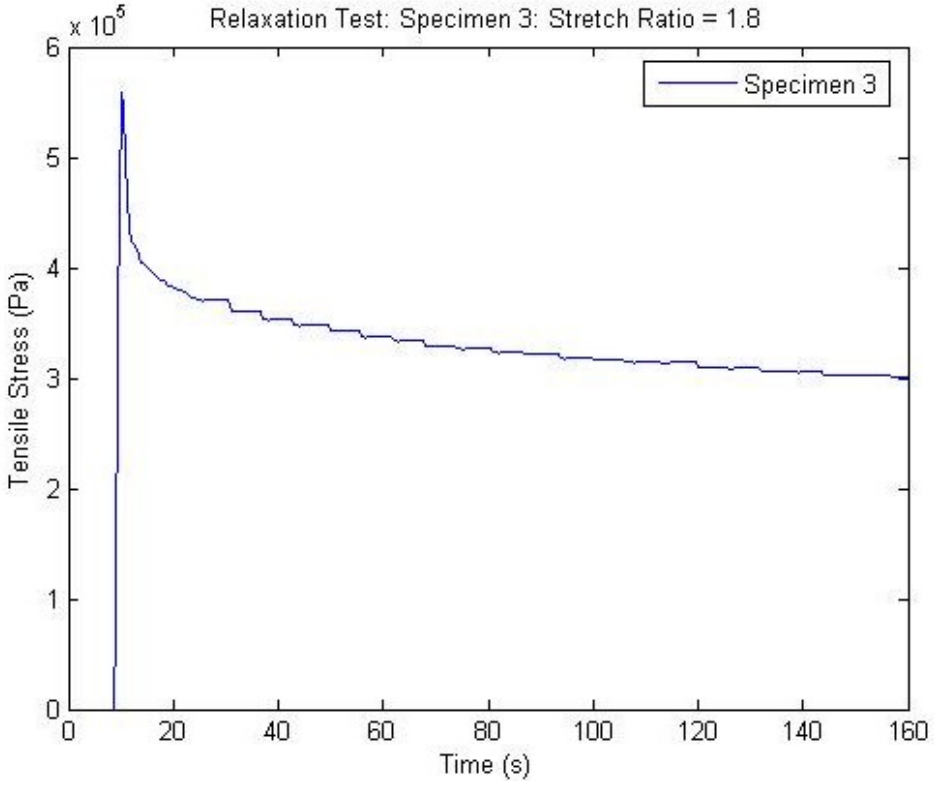

Figure 6.3 Relaxation test for specimen 3.

Among these three results, specimen 1 gave the best relaxation performance and thus was used for the viscoelastic property modeling. The Prony series could be used to describe the relaxation, which follows the following format:

$$E(t) = E_{\text{inf}} + \sum_{n=1}^{N} E_n \exp\left(-t / \tau_n\right),$$

where N is the number of orders. With $N = 1$, the function becomes exponential decaying function. With $N = 2$, the function becomes the relaxation function for Burger's model. The more orders used, the more precise the fit could be.

The results for $N = 1$, 2 and 3 were presented. The fitted parameters for the data are shown in Table 6.1, and the plotted curves are show in Figure 6.4.

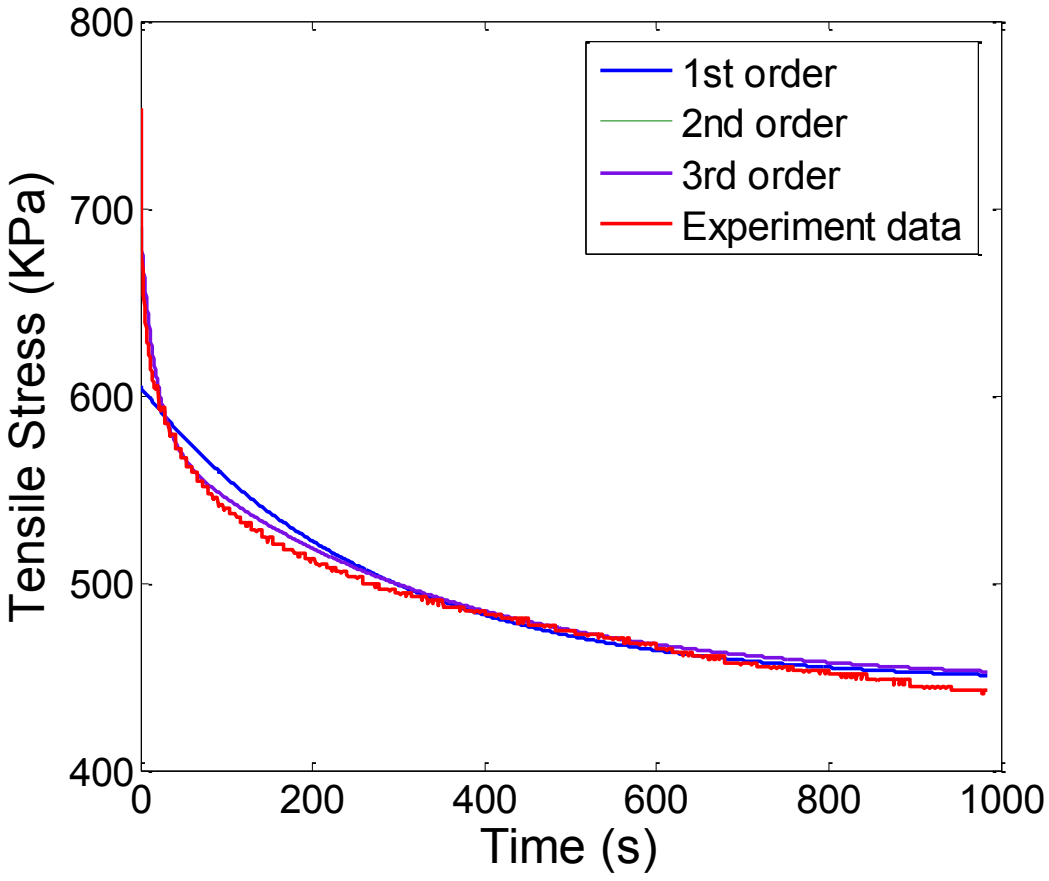

Figure 6.4 Comparison between fitting functions and experimental data.

Table 6.1 Data fitting results for different orders.

Order N	E_{inf}(Kpa)	E_1(Kpa)	τ_1(s)	E_2(Kpa)	τ_2(s)	E_3(Kpa)	τ_3(s)
1	446.54	158.3635	272.5819				
2	446.54	109.0560	16.9315	134.7136	320.1569		
3	446.54	109.0545	16.9324	67.3559	320.1318	67.3570	320.1849

First order fitting (as indicated by the blue curve) doesn't give a good fit. There are big differences in the beginning part of the curve. However, second order is much closer to the experimental data curve. Increasing one more order doesn't improve the precision too much. As shown in Figure 6.4, fitting with order number of 2 and fitting with order number of 3 are almost identical. Therefore, a second order fitting function for the tensile relaxation was used. The fitted tensile relaxation function was given as:

$$E(t) = 446.54 + 109.056\mathrm{e}^{-t/16.932} + 134.714\mathrm{e}^{-t/320.157} KPa$$

With $E(t)$ determined, the other time-depending functions for the contact problem and FEM simulation could be easily obtained as described in Chapter 4, Section 1.

5.2 Contact Problem

With the help of Matlab, it was possible to numerically calculate the dynamic stress tensor for any given point (x,y,z) in the half-space. The following slicing angles: 0° (vertical), 10°, 30°, 60° and 85° were selected. To evaluate the effects of slicing angle on the cutting process, Tresca's Criterion was introduced as a means to determine where the initiation of fracture occurred. The Tresca stress was calculated as $\tau = 0.5(\sigma_3 - \sigma_1)$, where σ_3 and σ_1 are the largest and least principal stresses. The critical shear stress τ_C of the biomaterial can be experimentally determined, and the prediction of failure can be made by simply comparing τ and τ_C. We are interested in stress distributions in the plane along

the blade cutting direction: *O-xz*, and the plane perpendicular to the blade: *O-yz*. The plots of the Tresca stress field in these two planes are shown in Figure 6.5 - 6.14. Noted is that, the stress has the same unit as the external force. In this paper, the units are *KPa.*

In the plane along the blade, the maximum Tresca stress occurs at the two ends of the blade ($x = a$ and $x = -a$). The magnitude increases when the slicing angle increases, meaning that the more tangential forces applied, the higher efficiency for the cutting process.

In Figure 6.5, the maximum Tresca stress under vertical loading is only about 0.04KPa, which is much lower compared with Figure 6.9, where the slicing angle is 85° and the maximum Tresca stress is about 0.11Kpa.

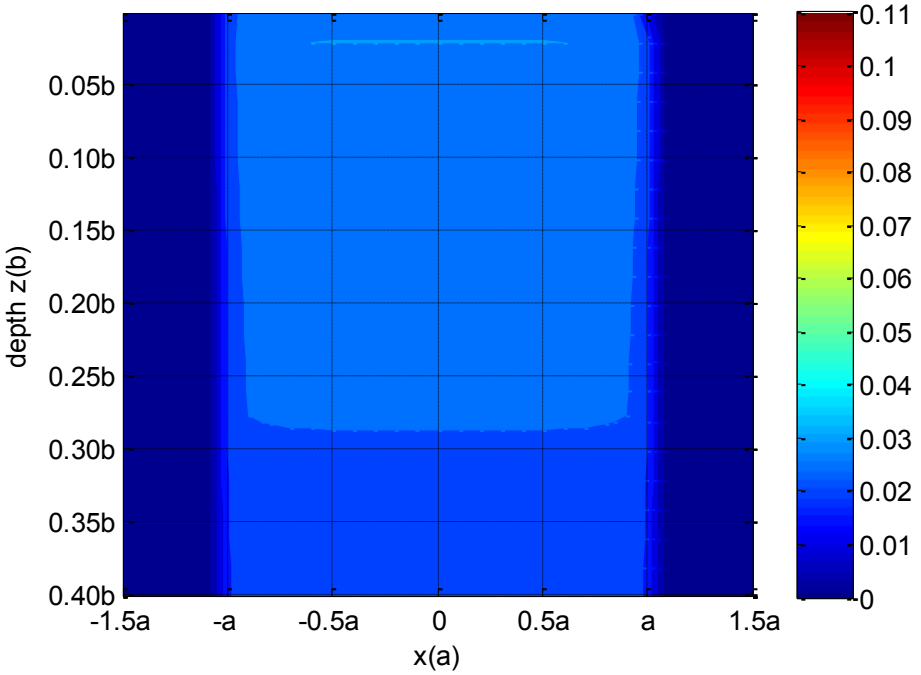

Figure 6.5Tresca stresses in O-xz plane under cutting angles of 0°.

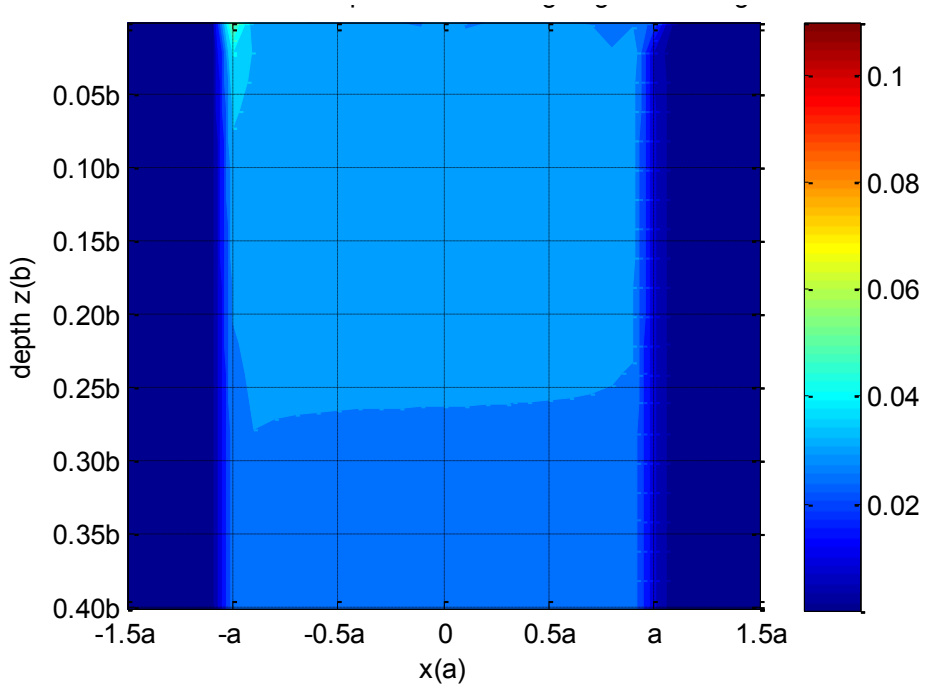

Figure 6.6 Tresca stresses in O-xz plane under cutting angles of 10°.

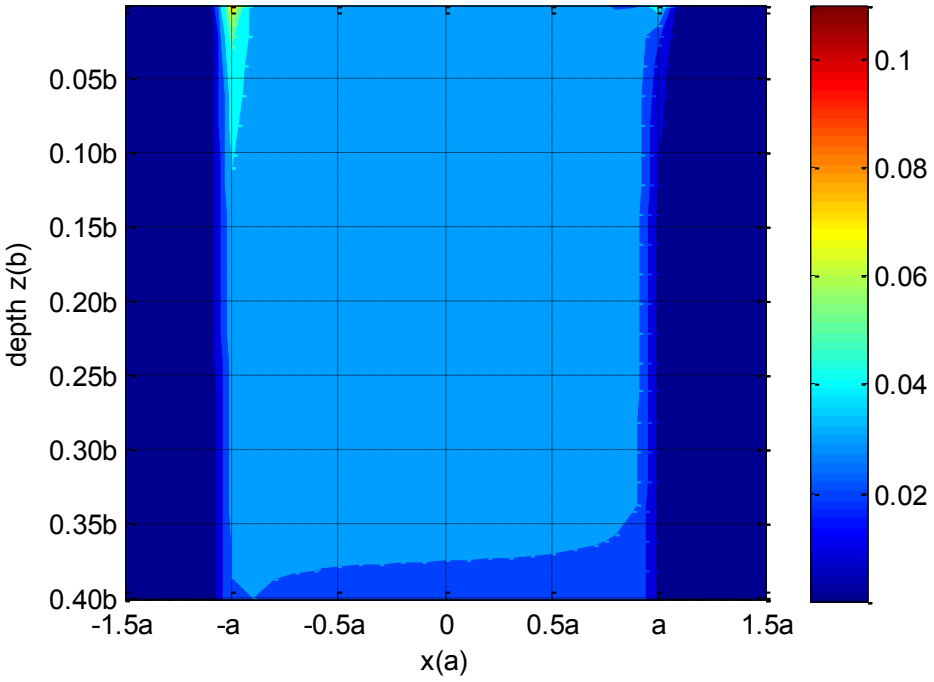

Figure 6.7 Tresca stresses in O-xz plane under cutting angles of 30°.

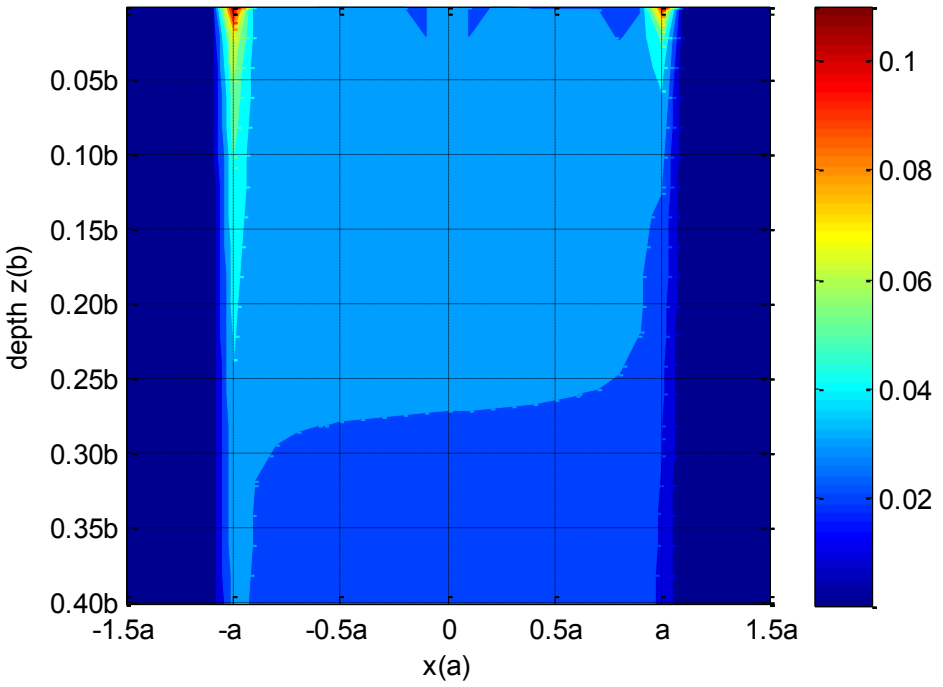

Figure 6.8 Tresca stresses in O-xz plane under cutting angles of 60°.

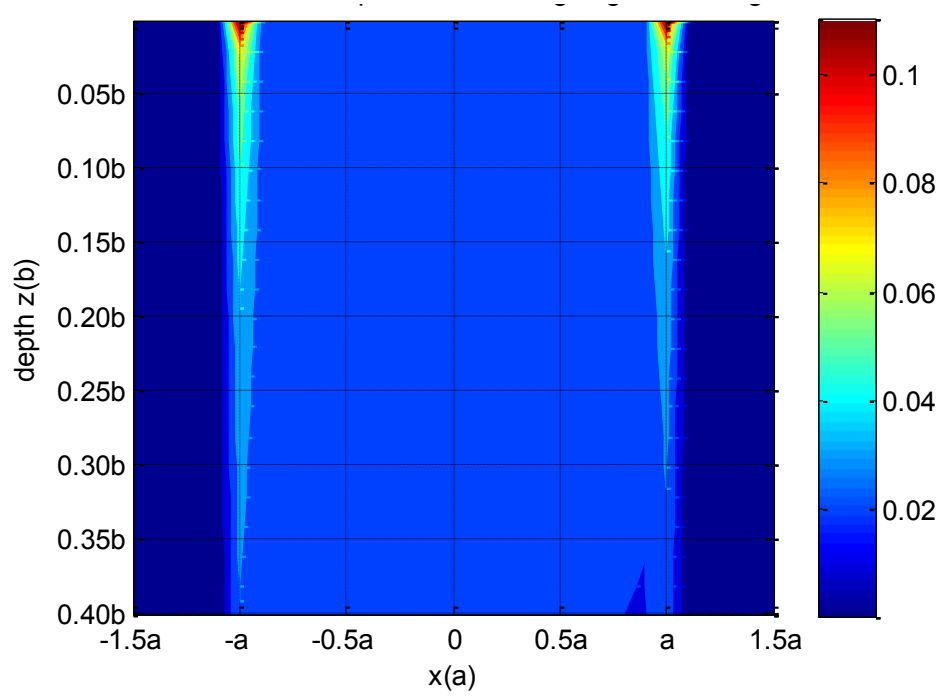

Figure 6.9 Tresca stresses in O-xz plane under cutting angles of 85°.

In the plane perpendicular to the blade, the maximum Tresca stress occurs when the slicing angle is 30° at about the depth of 0.1*b*, as shown in Figure 6.12. The magnitude shows a different pattern from in *O-xz* plane. Tresca stress reaches a peak value when the slicing angle is 30° and then drops when the slicing angle keeps increasing. Noted is that the maximum Tresca stress in *O-yz* plane is much lower than in *O-xz* plane, meaning the damage will not initiate in plane with constant $x = 0$, but in the two ends of the blade. Also, the maximum Tresca stress does not occur in the surface, but in a certain depth, as shown in Figure 6.12, meaning the damage will not directly initiate in the contacting surface. This observation shows the same pattern as in elastic bodies.

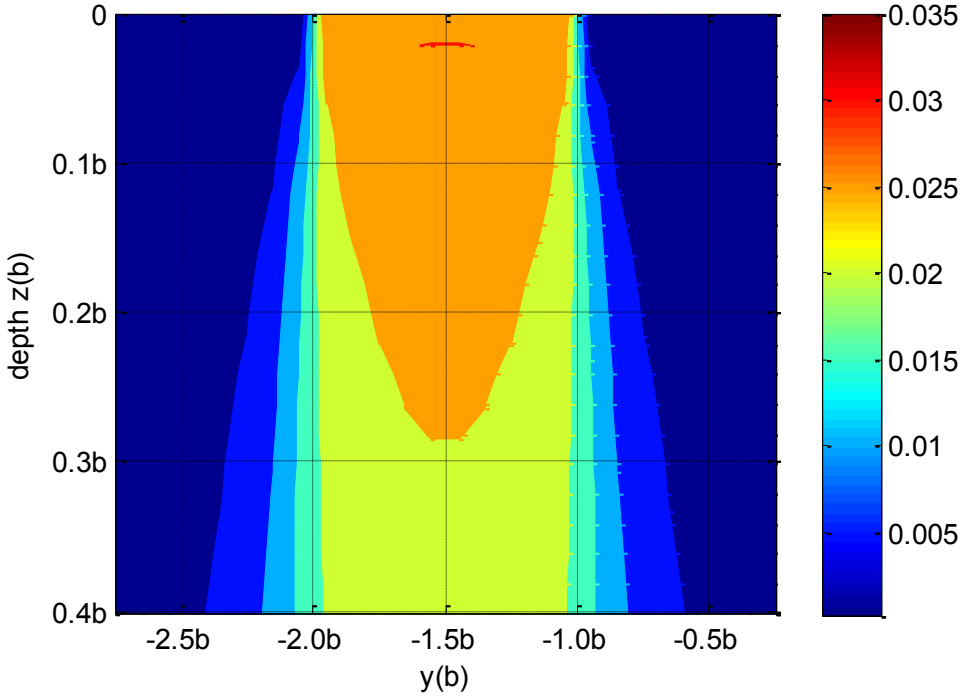

Figure 6.10 Tresca stresses in O-yz plane under cutting angles of 0°.

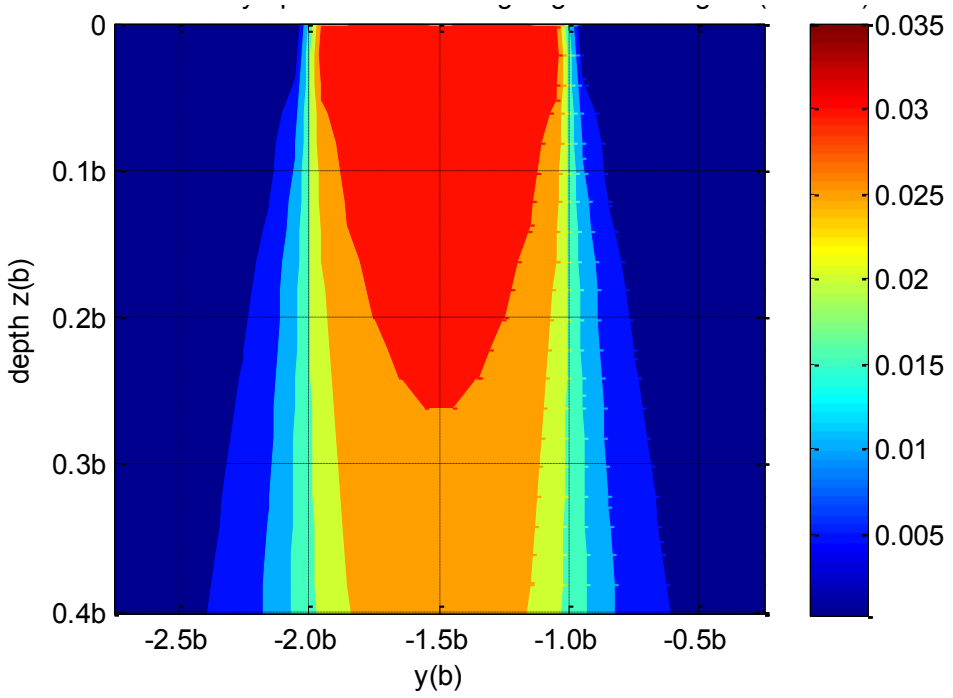

Figure 6.11 Tresca stresses in O-yz plane under cutting angles of 10°.

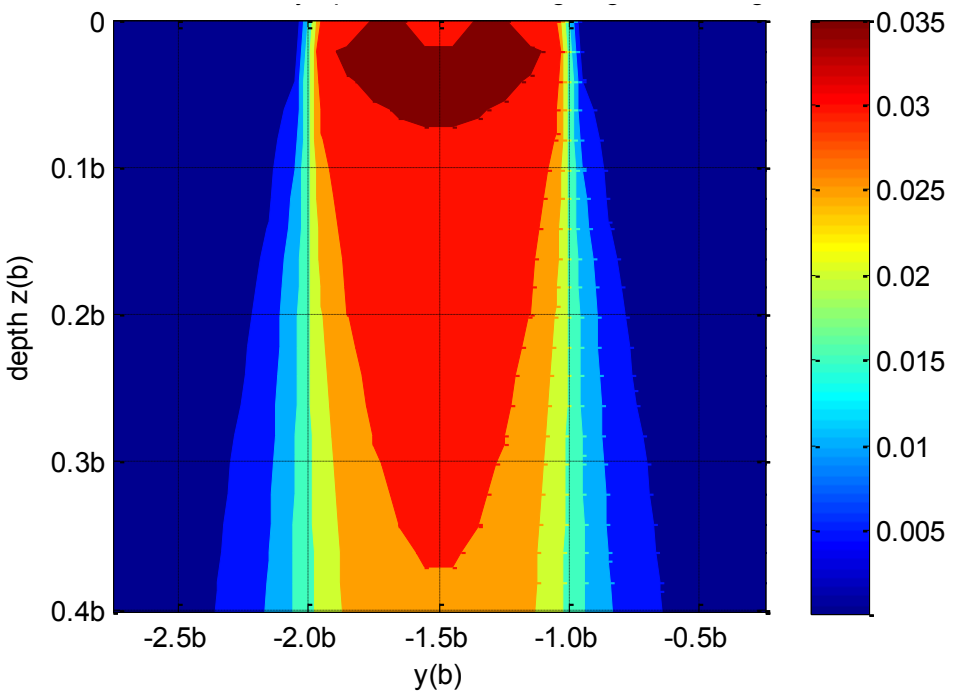

Figure 6.12 Tresca stresses in O-yz plane under cutting angles of 30°.

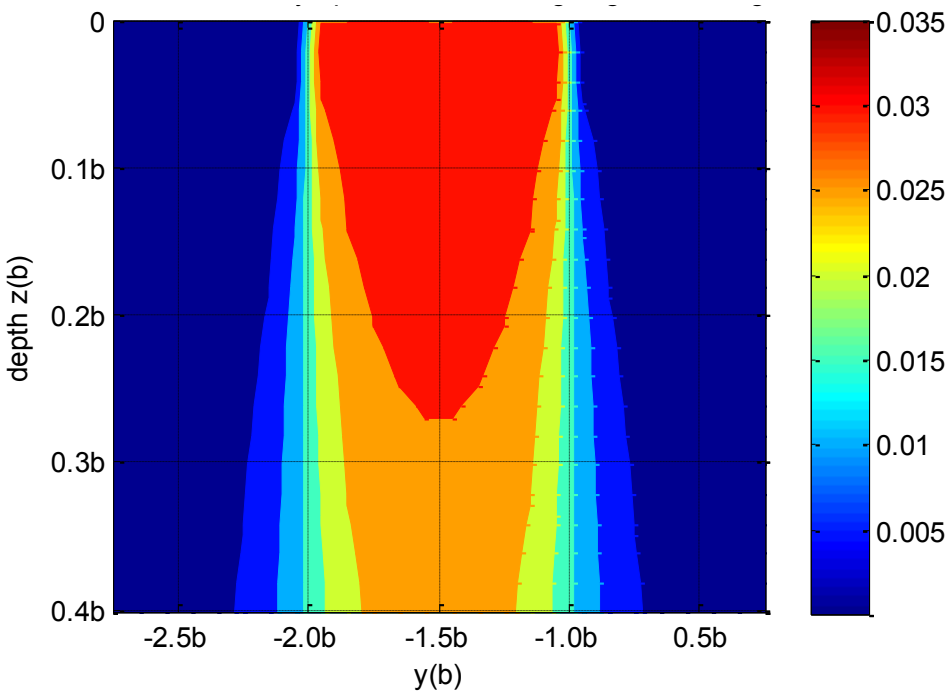

Figure 6.13 Tresca stresses in O-yz plane under cutting angles of 60°.

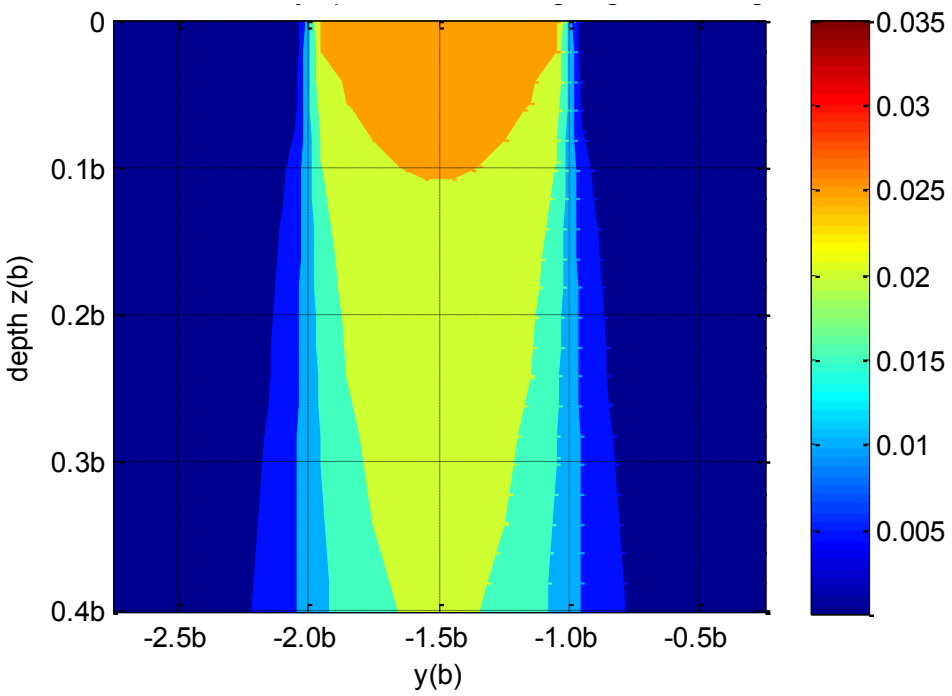

Figure 6.14 Tresca stresses in O-yz plane under cutting angles of 85°.

5.3 FEM Simulation

In the FEM simulation, the cutting process of a bi-layered viscoelastic biomaterial is examined (see Figure 3.10). The goal is to accurately re-visualize such a cutting activity which is ubiquitous in many fields. With the FEM cutting model validated, it can be applied to many applications such as surgical simulator design, or debone blade design. The key aspect of the simulation process is the dynamic force history on the blade, or the contact force between the two contact bodies as defined by ABAQUS. Many field variable monitors are set such as contacting forces, stress components, displacement, strain energy, fracture energy, kinematic energy, and so on.

In order to make this cutting model closer to application, the simulation put into the background of a computer-controlled robotic deboning process, in which a robotic controlled debone blade cuts into the bi-layered structure, the upper layer of the model represents the soft tissues and the lower layer of the model represents the bone. It is expected to use an intelligent robot to take place of the tradition manual work in a deboning process, of which the high repetitiveness incurs muscle fatigue to the workers and thus largely lowers the product yield and quality.

The logic for this design is, due to the existence of the bone (hard object), the blade force should reveal some pattern changes when it approaches the tissue-bone interface. Such a force pattern change could be used as a feedback signal to warn the computer of the close distance to the bone, and then to stop the blade proceeding. However, the phenomenal mechanical difference between soft tissues and bones is possibly to reduce the degree of the pattern change, and when the pattern change is small

in a certain degree, noise signals may severely distort the feedback algorithm and make it unable to work.

The simulations were also performed considering the cutting angle effects, with three different cutting angles of 0°, 30° and 60°. The normal forces and friction forces on the blade are plotted and shown in Figure 6.15 and Figure 6.16.

In both figures, the blade ran with a vertical velocity of 1cm/s and the total height of the soft tissue is 5cm; therefore, the blade cut into the bone at t = 5s. From the figure, it is obvious that all forces gained a big increase at t = 5s.

It was also noticed that the fracture initiation happened in the beginning at t = 0s when the blade cut into the body and created a rupture, which could be seen from the initial peak of the force pattern.

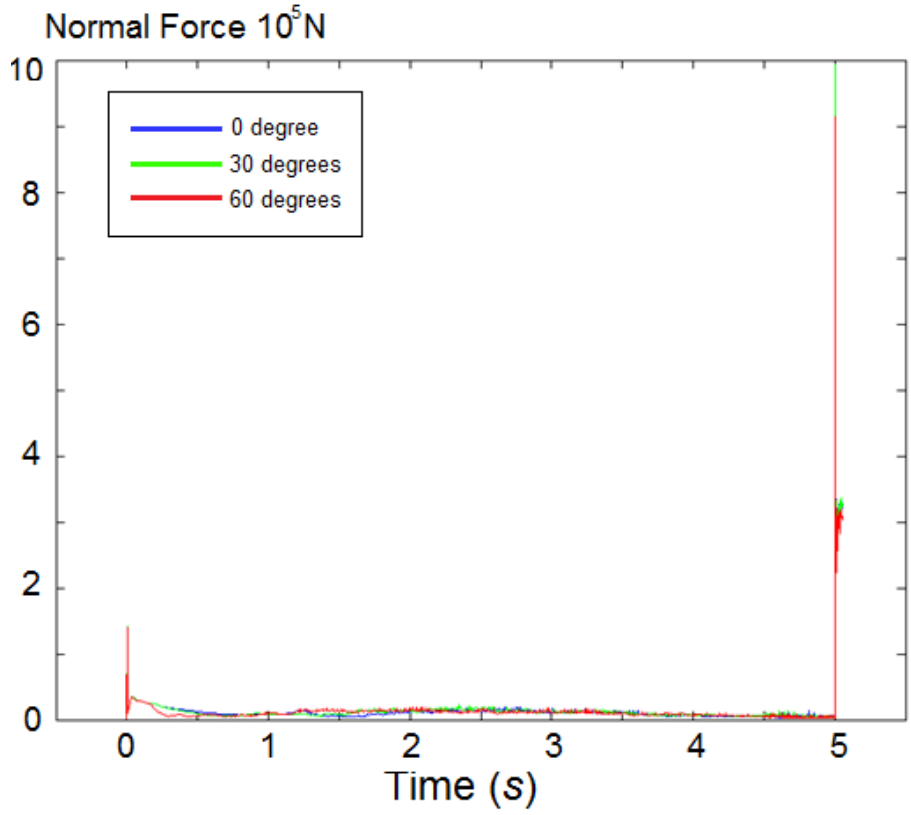

Figure 6.15 Normal forces with cutting angles of 0°, 30° and 60°.

There was barely any pattern change from the normal force history that could be visually recognized when the blade approaches the interface; therefore, normal forces don't seem to be a suitable control signal for the design.

Figure 6.16 shows the friction patterns for three different cutting angles. Note that the friction forces were much lower than in magnitude than normal forces, and there were many differences among these three curves. Compared with the normal forces, there were more changes during the middle part of the cutting process, from t = 1s to t = 4s. The friction forces showed an increase pattern from t = 1s to t = 2.5s and was then followed by a decrease from t = 2.5 to about t = 4s. It was noticed that, the larger the cutting angle, the lower the magnitude of the friction forces. These pattern changes could be used as potential indicators for the intelligent deboning robot design.

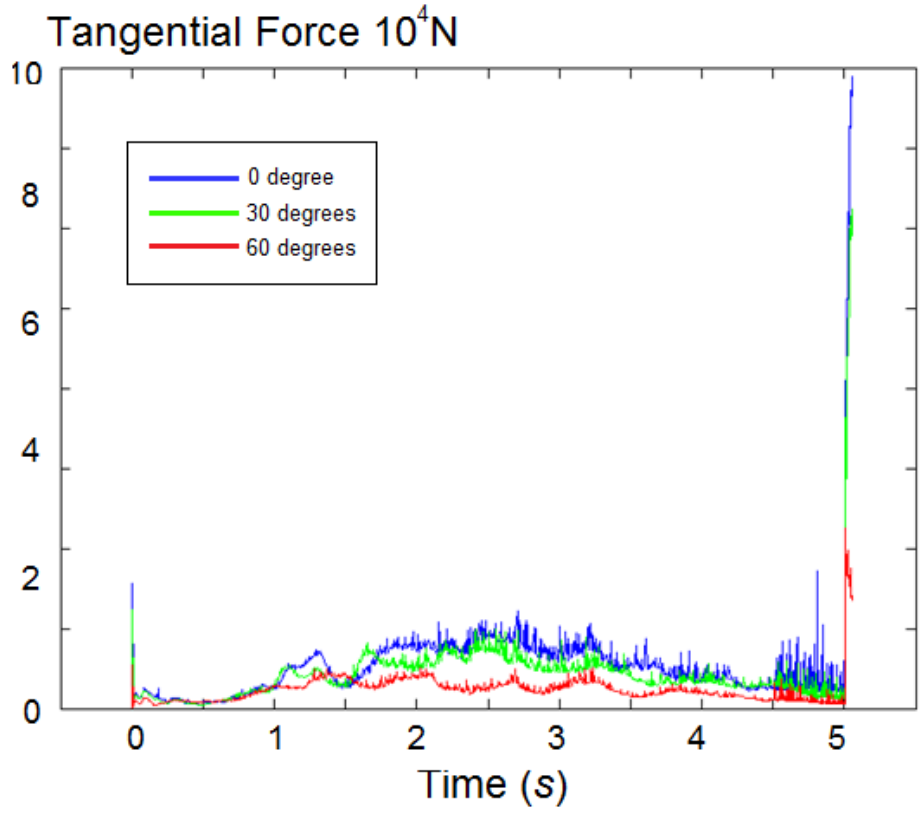

Figure 6.16 Tangential forces with cutting angles of 0°, 30° and 60°.

Another fact noted is shown in Figure 6.17, in which the friction forces at the rupture initiation are plotted. It was noticed that the friction forces needed for the initial rupture decrease with the cutting angle. The larger the cutting angle, the smaller the friction force needed. This may be an evidence to explain why it's much easier to cut materials with a slicing effort than pure normal pressing.

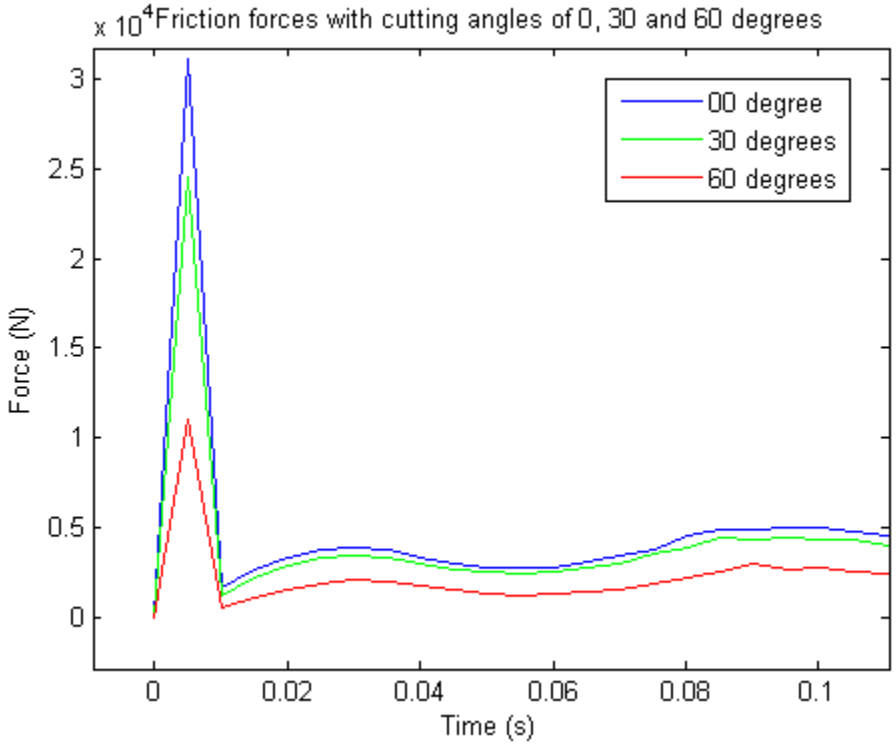

Figure 6.17 Friction forces during initial rupture.

CHAPTER VI CONCLUSIONS AND FUTURE WORK

6.1 Conclusions

In this study, a whole viscoelastic material cutting process model was successfully developed with either analytic solutions or FEM simulations. Experiments were conducted to provide the necessary parameters.

In the viscoelastic material modeling experiment, relaxation tests were successfully performed using an EPSON robot. Ligaments dissected from chicken wings were used as specimen. The relaxation test provided the tensile relaxation modulus as the viscoelastic mechanical properties of the biomaterials. The experimental data were theoretically fitted into a second order Burgers model.

In the stage I modeling, an analytical model was developed by considering the contact of a blade with a viscoelastic half-space. The effects of blade on the body were considered as distributed pressure on the upper surface of the half-space. The solutions to the stress and displacement fields were computed by introducing the correspondence principle and by applying a numerical strategy for the surface integration. Based on the results, stress components in the half-space can be both analytically and numerically calculated for any plane of interest, such as plane *O-xz*, which is parallel to the direction of the tangential forces, or plane *O-yz*, which is perpendicular to the tangential forces. Knowing the stress tensor $[\sigma]_{3x3}$, it is able to obtain the principal stress and predict the failure using Tresca's criterion, which requires the calculation of maximum shear stress.

Tresca stresses were plotted under different cutting angles, and the effect of cutting angle on Tresca stress was examined. It was noticed that the Tresca stress decreased with the increase of cutting angle, meaning that the cutting process would be much easier to perform with more shear efforts.

In the stage II modeling, an ABAQUS bi-layered structure was used to represent the soft-tissue and bone structure. The blade was modeled as a rigid body, the soft tissue was modeled as a linear isotropic homogenous viscoelastic material, and the bone was modeled as an elastic material with very high Young's Modulus. The deboning blade design was discussed based on the results. The results showed some mechanical facts that are reasonable to imagine in real applications. The normal forces applied on the blade didn't change too much in dynamic pattern when the blade approached the interface. However, the friction forces on the blade did show some uncommon patterns along with the cutting depth. Thus it provided a theoretically sound method to design an intelligent deboning robot to deal with the muscle fatigue problem encountered during food processing.

6.2 Future Work

This cutting model introduced in this research does have some limits, and thus many improvements could be done to make the model more accurate and reliable.

First, the geometry of the models is simple. In the contact problem modeling, the semi-infinite space was used to represent the body; however, the model should be confined in a finite space. The assumption was made to support such a model that once the boundary region of the contact stress was comparatively smaller than the real

biomaterial body geometry, then the model could be viewed as an infinite half-space. However, further studies remain to be done to verify such an assumption. In the FEM model, the bi-layered structure was modeled using two rectangular blocks, which is not realistic for a complicate biological structure, and thus potential errors in estimating the blade force may exist. Further work could be done in precisely reconstructing the geometry. Tools such as CT scan could be used for non-invasive detection and reconstruction. Paraffin Section methods could be used to treat the tissue or ligament specimen when they are too soft for catching the geometric characteristics.

Second, the assumptions of linear homogenous isotropic material are very ideal. Though such an assumption was widely used in many bio-material researchers, it is still far away from acceptable. Most soft biological tissues demonstrate non-linear properties, in which the stress and strain relationship doesn't follow Hooke's Law. Without the linearity, superposition as we used in stage I modeling could not be used. Many researchers have employed the hyperelastic model to address such a problem. The hyperelastic materials show complete elasticity but have a nonlinear stress-strain curve. Energy based methods are used to describe its mechanical properties. The validation of the homogenous or isotropic assumptions depends on the specific material to examine. Some biological tissues, for example, liver tissues or skin tissues, show good homogenous and isotropic properties, while some others, for example, cells in vessel wall, show strong direction-related mechanical property due to its particular biological structure. In the FEM simulation in this research, the muscle tissues were used as the biomaterial. Muscle tissues show direction-dependent mechanical properties, and thus

improvement for this study could be done in determining the direction-related viscoelastic material constants.

In the experiments, the assumption of constant bulk modulus was made to simplify the calculation. It was an acceptable assumption especially when the decaying amount of tensile relaxation is much greater than the bulk relaxation. However, future work could be done to precisely measure the viscoelastic behavior of biological tissues in any two of the tensile relaxation modulus, bulk relaxation modulus and shear relaxation modulus. Though experiment designs to obtain these moduli in soft biological tissues are very difficult, some references have provided useful tools for this problem, such as finding the time-dependent Poisson's ratio as an alternative of the shear or bulk relaxation modulus.

REFERENCES

Abdel-Wahab AA, Alam K, Silberschmidt VV. 2011. Analysis of anisotropic viscoelastoplastic properties of cortical bone tissues. Journal of the Mechanical Behavior of Biomedical Materials 4(5):807-820.

Adolph M, Mesquita E, Carvalho ER, Romanini E. 2007. Numerically evaluated displacement and stress solutions for a 3D viscoelastic half space subjected to a vertical distributed surface stress loading using the Radon and Fourier transforms. Communications in Numerical Methods in Engineering 23(8):787-804.

Atkins AG, Xu X, Jeronimidis G. 2004. Cutting, by 'pressing and slicing,' of thin floppy slices of materials illustrated by experiments on cheddar cheese and salami. Journal of Materials Science 39(8):2761-2766.

Bouchbinder E, Brener EA. 2011. Viscoelastic fracture of biological composites. Journal of the Mechanics and Physics of Solids 59(11):2279-2293.

Brown T, James SJ, Purnell GL. 2005. Cutting forces in foods: experimental measurements. Journal of Food Engineering 70(2):165-170.

Cheng Y-T, Yang F. 2009. Obtaining shear relaxation modulus and creep compliance of linear viscoelastic materials from instrumented indentation using axisymmetric indenters of power-law profiles. Journal of Materials Research 24(10):3013-3017.

Cordes JA, Chang AT, Charvet JL. 1998. Predicting fracture from the tensile properties of a composite biomaterial. Composites Part a-Applied Science and Manufacturing 29(12):1475-1480.

DeFrate LE, Li G. 2007. The prediction of stress-relaxation of ligaments and tendons using the quasi-linear viscoelastic model. Biomechanics and Modeling in Mechanobiology 6(4):245-251.

Dempsey PG, McGorry RW. 2004. Investigation of a pork shoulder deboning operation. Journal of Occupational and Environmental Hygiene 1(3):167-172.

Dhar PR, Zu JW. 2007. Design of a resonator device for in vivo measurement of regional tissue viscoelasticity. Sensors and Actuators a-Physical 133(1):45-54.

Dydo JR, Busby HR. 1995. ELASTICITY SOLUTIONS FOR CONSTANT AND LINEARLY VARYING LOADS APPLIED TO A RECTANGULAR SURFACE PATCH ON THE ELASTIC HALF-SPACE. Journal of Elasticity 38(2):153-163.

Gamonpilas C, Charalambides MN, Williams JG. 2009. Determination of large deformation and fracture behaviour of starch gels from conventional and wire cutting experiments. Journal of Materials Science 44(18):4976-4986.

Geerligs M, Peters GWM, Ackermans PAJ, Oomens CWJ, Baaijens FPT. 2008. Linear viscoelastic behavior of subcutaneous adipose tissue. Biorheology 45(6):677-688.

Geubelle PH. 1997. A numerical method for elastic and viscoelastic dynamic fracture problems in homogeneous and bimaterial systems. Computational Mechanics 20(1-2):20-25.

Gokgol C, Basdogan C, Canadinc D. 2012. Estimation of fracture toughness of liver tissue: Experiments and validation. Medical Engineering & Physics 34(7):882-891.

Jacquemoud C, Bruyere-Garnier K, Coret M. 2007. Methodology to determine failure characteristics of planar soft tissues using a dynamic tensile test. Journal of Biomechanics 40(2):468-475.

Johnson K.L., *Contact Mechanics*, Cambridge University Press (1985)

Kamyab I, Chakrabarti S, Williams JG. 1998. Cutting cheese with wire. Journal of Materials Science 33(11):2763-2770.

Kim J, Lee HS, Kim N. 2010. Determination of Shear and Bulk Moduli of Viscoelastic Solids from the Indirect Tension Creep Test. Journal of Engineering Mechanics-Asce 136(9):1067-1075.

Koop BE, Lewis JL. 2003. A model of fracture testing of soft viscoelastic tissues. Journal of Biomechanics 36(4):605-608.

Kundu S, Crosby AJ. 2009. Cavitation and fracture behavior of polyacrylamide hydrogels. Soft Matter 5(20):3963-3968.

Lakes R.S., *Viscoelastic Solids*, CRC Press (1999)

Li J, Berger EJ. 2003. A semi-analytical approach to three-dimensional normal contact problems with friction. Computational Mechanics 30(4):310-322.

Li JS, Berger EJ. 2001. A Boussinesq-Cerruti solution set for constant and linear distribution of normal and tangential load over a triangular area. Journal of Elasticity 63(2):137-151.

Love A.E.H., The stress produced in a semi-infinite solid by pressure on part of the boundary.*Phil. Trans. Roy. Soc. London* **A228** (1929) 377.

Mahvash M, Dupont PE. 2010a. Mechanics of Dynamic Needle Insertion into a Biological Material. Ieee Transactions on Biomedical Engineering 57(4):934-943.

Mahvash M, Dupont PE. 2010b. Mechanics of Dynamic Needle Insertion into a Biological Material. Ieee Transactions on Biomedical Engineering 57(4):934-943.

Mahvash M, Voo LM, Kim D, Jeung K, Wainer J, Okamura AM. 2008. Modeling the forces of cutting with scissors. Ieee Transactions on Biomedical Engineering 55(3):848-856.

Mann KA, Damron LA. 2002. Predicting the failure response of cement-bone constructs using a non-linear fracture mechanics approach. Journal of Biomechanical Engineering-Transactions of the Asme 124(4):462-470.

McCarthy CT, Hussey M, Gilchrist MD. 2007. On the sharpness of straight edge blades in cutting soft solids: Part I - indentation experiments. Engineering Fracture Mechanics 74(14):2205-2224.

Mesquita E, Romanini E, Labaki J. 2012. Stationary Dynamic Displacement Solutions for a Rectangular Load Applied within a 3D Viscoelastic Isotropic Full Space-Part I: Formulation. Mathematical Problems in Engineering.

Nasseri S, Bilston LE, Phan-Thien N. 2002. Viscoelastic properties of pig kidney in shear, experimental results and modelling. Rheologica Acta 41(1-2):180-192.

Natali AN, Carniel EL, Pavan PG, Sander FG, Dorow C, Geiger M. 2008. A visco-hyperelastic-damage constitutive model for the analysis of the biomechanical response of the periodontal ligament. Journal of Biomechanical Engineering-Transactions of the Asme 130(3).

Nikas GK. 2006. Boussinesq-Cerruti functions and a simple technique for substantial acceleration of subsurface stress computations in elastic half-spaces. Proceedings of the Institution of Mechanical Engineers Part J-Journal of Engineering Tribology 220(J1):19-28.

Oza A, Vanderby R, Lakes RS. 2006. Generalized solution for predicting relaxation from creep in soft tissue: Application to ligament. International Journal of Mechanical Sciences 48(6):662-673.

Pena E, Pena JA, Doblare M. 2008. On modelling nonlinear viscoelastic effects in ligaments. Journal of Biomechanics 41(12):2659-2666.

Pioletti DP, Rakotomanana LR. 2000. On the independence of time and strain effects in

the stress relaxation of ligaments and tendons. Journal of Biomechanics 33(12):1729-1732.

Reilly GA, McCormack BAO, Taylor D. 2004. Cutting sharpness measurement: a critical review. Journal of Materials Processing Technology 153:261-267.

Reyssat E, Tallinen T, Le Merrer M, Mahadevan L. 2012. Slicing Softly with Shear. Physical Review Letters 109(24).

Schepers W, Savidis S, Kausel E. 2010. Dynamic stresses in an elastic half-space. Soil Dynamics and Earthquake Engineering 30(9):833-843.

Selvaduari APS. 2000. Boussinesq's problem for an elastic half-space reinforced with a rigid disk inclusion. Mathematics and Mechanics of Solids 5(4):483-499.

Shergold OA, Fleck NA. 2004. Mechanisms of deep penetration of soft solids, with application to the injection and wounding of skin. Proceedings of the Royal Society of London Series a-Mathematical Physical and Engineering Sciences 460(2050):3037-3058.

Shergold OA, Fleck NA. 2005. Experimental investigation into the deep penetration of soft solids by sharp and blunt punches, with application to the piercing of skin. Journal of Biomechanical Engineering-Transactions of the Asme 127(5):838-848.

Subit D, Chabrand P, Masson C. 2009. A micromechanical model to predict damage and failure in biological tissues. Application to the ligament-to-bone attachment in the human knee joint. Journal of Biomechanics 42(3):261-265.

Svec O.J. and Gladwell G.M.L., An explicit Boussinesq solution for a polynomial distribution of pressure over a triangular region. *J. Elasticity* **1** (1971) 167–170.

Sy Tuan N, Dormieux L, Le Pape Y, Sanahuja J. 2011. A Burger Model for the Effective Behavior of a Microcracked Viscoelastic Solid. International Journal of Damage Mechanics 20(8):1116-1129.

Szabo RL, Radwin RG, Henderson CJ. 2001. The influence of knife dullness on poultry processing operator exertions and the effectiveness of periodic knife steeling. Aihaj 62(4):428-433.

Talybly LK. 2010. Boussinesq's viscoelastic problem on normal concentrated force on a half-space surface. Mechanics of Time-Dependent Materials 14(3):253-259.

Valtorta D, Mazza E. 2005. Dynamic measurement of soft tissue viscoelastic properties with a torsional resonator device. Medical Image Analysis 9(5):481-490.

Vandamme M, Ulm FJ. 2006. Viscoelastic solutions for conical indentation. International

Journal of Solids and Structures 43(10):3142-3165.

Yamashita H, Matsumiya K, Masamune K, Liao H, Chiba T, Dohi T. 2008. Miniature bending manipulator for fetoscopic intrauterine laser therapy to treat twin-to-twin transfusion syndrome. Surgical Endoscopy and Other Interventional Techniques 22(2):430-435.

Yun Peng and Debao Zhou**,** *Formulation of the Stress Distribution Due to a Concentrated Force Acting on the Boundary of Viscoelastic Half-Space*, Journal of Computations & Modelling, vol.2, no.4, 2012, 51-74, 2012.

Zhang C.Y., *Viscoelastic Fracture Mechanics (Chinese)*, Hua zhong li gong ta xue chu ban she (1984).

Zhang W, Chen HY, Kassab GS. 2007. A rate-insensitive linear viscoelastic model for soft tissues. Biomaterials 28(24):3579-3586.

Zhou D, McMurray G. 2010. Modeling of blade sharpness and compression cut of biomaterials. Robotica 28:311-319.

APPENDIX

MATLAB CODES FOR NUMERICAL METHOD

This function calculates the surface integration of first stress component in xx direction under vertical pressure

```
************************************************
function fxx1 = fxx1 (x,y,z)
global a b;
fun = @(p,q) 3.*(x-p).^2.*z./sqrt((x-p).^2 + (y-
q).^2+z.^2).^5;
fxx1 = dblquad(fun,-a,a,-b,b)/(2*pi);
end
```

This function calculates the surface integration of second stress component in xx direction under vertical pressure

```
************************************************
function fxx2 = fxx2 (x,y,z)
global a b;
fun = @(p,q) ((x-p).^2-(y-q).^2)./sqrt((x-p).^2+(y-
q).^2+z.^2)./sqrt((x-p).^2+(y-q).^2).^2./(sqrt((x-p).^2+(y-
q).^2+z.^2)+z)+ (y-q).^2.*z./sqrt((x-p).^2+(y-
q).^2+z.^2).^3./sqrt((x-p).^2+(y-q).^2).^2;

if (x^2>a^2)&&(y^2>b^2)
      fxx2 = dblquad(fun,-a,a,-b,b)/(2*pi);
else
      epson = 1e-6;
      part1 = dblquad(fun,-a,a,y+epson,b);
            part2 = dblquad(fun,-a,x-epson,-b,y+epson);
            part3 = dblquad(fun,x+epson,a,-b,y+epson);
            part4 = dblquad(fun,x-epson,x+epson,-b,y-epson);
      fxx2 = (part1 + part2 + part3 + part4)/(2*pi);
end
end
```

This function calculates the surface integration of the stress component in zz direction under vertical pressure

```
************************************************
function fzz1 = fzz1 (x,y,z)
global a b;
fun = @(p,q) 3.*z.^3./sqrt((x-p).^2 + (y-q).^2+z.^2).^5;
fzz1 = dblquad(fun,-a,a,-b,b)/(2*pi);
end
```

This function calculates the surface integration of first stress component in xz direction under vertical pressure

```
************************************************
function fxz1 = fxz1 (x,y,z)
global a b;
fun = @(p,q) 3.*(x-p).*z.^2./sqrt((x-p).^2 + (y-
q).^2+z.^2).^5;
fxz1 = dblquad(fun,-a,a,-b,b)/(2*pi);
end
```

This function calculates the surface integration of first stress component in yz direction under vertical pressure

```
************************************************
function fyz1 = fyz1 (x,y,z)
global a b;
fun = @(p,q) 3.*(y-q).*z.^2./sqrt((x-p).^2 + (y-
q).^2+z.^2).^5;
fyz1 = dblquad(fun,-a,a,-b,b)/(2*pi);
end
```

This function calculates the surface integration of first stress component in yy direction under vertical pressure

```
************************************************
function fyy1 = fyy1 (x,y,z)
global a b;
fun = @(p,q) 3.*(y-q).^2.*z./sqrt((x-p).^2 + (y-
q).^2+z.^2).^5;
fyy1 = dblquad(fun,-a,a,-b,b)/(2*pi);
end
```

This function calculates the surface integration of second stress component in yy direction under vertical pressure

```
************************************************
function fyy2 = fyy2 (x,y,z)
global a b;
fun = @(p,q) ((y-q).^2-(x-p).^2)./sqrt((x-p).^2+(y-
q).^2+z.^2)./sqrt((x-p).^2+(y-q).^2).^2./(sqrt((x-p).^2+(y-
q).^2+z.^2)+z) + (x-p).^2.*z./sqrt((x-p).^2+(y-
q).^2+z.^2).^3./sqrt((x-p).^2+(y-q).^2).^2;

if (x^2>a^2)&&(y^2>b^2)
   fyy2 = dblquad(fun,-a,a,-b,b)/(2*pi);
else
   epson = 1e-6;
   part1 = dblquad(fun,-a,a,y+epson,b);
   part2 = dblquad(fun,-a,x-epson,-b,y+epson);
   part3 = dblquad(fun,x+epson,a,-b,y+epson);
   part4 = dblquad(fun,x-epson,x+epson,-b,y-epson);
   fyy2 = (part1 + part2 + part3 + part4)/(2*pi);
end
end
```

This function calculates the surface integration of first stress component in xy direction under vertical pressure

```
************************************************
function fxy1 = fxy1 (x,y,z)
global a b;
fun = @(p,q) 3.*(x-p).*(y-q).*z./sqrt((x-p).^2 + (y-
q).^2+z.^2).^5;
fxy1 = dblquad(fun,-a,a,-b,b)/(2*pi);
end
```

This function calculates the surface integration of second stress component in xy direction under vertical pressure

```
************************************************
function fxy2 = fxy2 (x,y,z)
global a b;
fun = @(p,q) (x-p).*(y-q)./sqrt((x-p).^2+(y-
q).^2+z.^2)./sqrt((x-p).^2+(y-q).^2).^2./(sqrt((x-p).^2+(y-
q).^2+z.^2)+z) + (x-p).*(y-q).*z./sqrt((x-p).^2+(y-
q).^2+z.^2).^3./sqrt((x-p).^2+(y-q).^2).^2;

if (x^2>a^2)&&(y^2>b^2)
      fxy2 = dblquad(fun,-a,a,-b,b)/(2*pi);
else
      epson = 1e-6;
      part1 = dblquad(fun,-a,a,y+epson,b);
      part2 = dblquad(fun,-a,x-epson,-b,y+epson);
      part3 = dblquad(fun,x+epson,a,-b,y+epson);
      part4 = dblquad(fun,x-epson,x+epson,-b,y-epson);
      fxy2 = (part1 + part2 + part3 + part4)/(2*pi);
end
end
```

This function calculates the surface integration of first stress component in xx direction under tangential shear stress
****
```
function sxx1 = sxx1 (x,y,z)
global a b;
fun = @(p,q) -3.*(x-p).^3./sqrt((x-p).^2+(y-q).^2+z.^2).^5;
sxx1 = dblquad(fun,-a,a,-b,b)/(2*pi);
end
```

This function calculates the surface integration of second stress component in xx direction under tangential shear stress
****
```
function sxx2 = sxx2 (x,y,z)
global a b;
fun = @(p,q) (x-p)./sqrt((x-p).^2+(y-q).^2+z.^2).^3./(sqrt((x-p).^2+(y-q).^2+z.^2)+z).^2.*(sqrt((x-p).^2+(y-q).^2+z.^2).^2-(y-q).^2-2.*sqrt((x-p).^2+(y-q).^2+z.^2).*(y-q).^2./(sqrt((x-p).^2+(y-q).^2+z.^2)+z));
sxx2 = dblquad(fun,-a,a,-b,b)/(2*pi);
end
```

This function calculates the surface integration of first stress component in yy direction under tangential shear stress
****
```
function syy1 = syy1 (x,y,z)
global a b;
fun = @(p,q) -3.*(x-p).*(y-q).^2./sqrt((x-p).^2+(y-q).^2+z.^2).^5;
syy1 = dblquad(fun,-a,a,-b,b)/(2*pi);
end
```

This function calculates the surface integration of second stress component in yy direction under tangential shear stress
****
```
function syy2 = syy2 (x,y,z)
global a b;
fun = @(p,q) (x-p)./sqrt((x-p).^2+(y-q).^2+z.^2).^3./(sqrt((x-p).^2+(y-q).^2+z.^2)+z).^2.*(3.*sqrt((x-p).^2+(y-q).^2+z.^2).^2-(x-p).^2-2.*sqrt((x-p).^2+(y-q).^2+z.^2).*(x-p).^2./(sqrt((x-p).^2+(y-q).^2+z.^2)+z));
syy2 = dblquad(fun,-a,a,-b,b)/(2*pi);
end
```

This function calculates the surface integration of the stress component in zz direction under tangential shear stress
****
```
function szz1 = szz1 (x,y,z)
global a b;
fun = @(p,q) -3.*(x-p).*z.^2./sqrt((x-p).^2+(y-q).^2+z.^2).^5;
szz1 = dblquad(fun,-a,a,-b,b)/(2*pi);
end
```

This function calculates the surface integration of the stress component in xz direction under tangential shear stress
****
```
function sxz1 = sxz1 (x,y,z)
global a b;
fun = @(p,q) -3.*(x-p).^2.*z./sqrt((x-p).^2+(y-q).^2+z.^2).^5;
sxz1 = dblquad(fun,-a,a,-b,b)/(2*pi);
end
```

This function calculates the surface integration of first stress component in xy direction under tangential shear stress
****
```
function sxy1 = sxy1 (x,y,z)
global a b;
fun = @(p,q) -3.*(x-p).^2.*(y-q)./sqrt((x-p).^2+(y-q).^2+z.^2).^5;
sxy1 = dblquad(fun,-a,a,-b,b)/(2*pi);
end
```

This function calculates the surface integration of second stress component in xy direction under tangential shear stress
****
```
function sxy2 = sxy2 (x,y,z)
global a b;
fun = @(p,q) (y-q)./sqrt((x-p).^2+(y-q).^2+z.^2).^3./(sqrt((x-p).^2+(y-q).^2+z.^2)+z).^2.*(-sqrt((x-p).^2+(y-q).^2+z.^2).^2+(x-p).^2+2.*sqrt((x-p).^2+(y-q).^2+z.^2).*(x-p).^2./(sqrt((x-p).^2+(y-q).^2+z.^2)+z));
sxy2 = dblquad(fun,-a,a,-b,b)/(2*pi);
end
```

This function calculates the surface integration of the stress component in yz direction under tangential shear stress
****
```
function syz1 = syz1 (x,y,z)
global a b;
fun = @(p,q) -3.*(x-p).*(y-q).*z./sqrt((x-p).^2+(y-q).^2+z.^2).^5;
syz1 = dblquad(fun,-a,a,-b,b)/(2*pi);
end
```

```
This function calculates all stress components on xoz plane
and generate the plots
************************************************
function plot_xoz (x_min, x_step, x_max, z_min, z_step,
z_max, t_step, angle)
% Entries are the boundaries for x and z
% z_min cannot be 0, or "divided by 0" will occur
% y is set to be zero on XOZ plane

global t_total
ct = 30; % number of contours
Nx = ceil((x_max - x_min)/(x_step));
Nz = ceil((z_max - z_min)/(z_step));
[xx,zz] = meshgrid(x_min:x_step:x_max,
z_min:z_step:z_max);

%------------Calculating the spatial terms-------------------------%
% Initialization
Fxx1(Nz+1,Nx+1)=0;
Fxx2(Nz+1,Nx+1)=0;
Fyy1(Nz+1,Nx+1)=0;
Fyy2(Nz+1,Nx+1)=0;
Fzz1(Nz+1,Nx+1)=0;
Fyz1(Nz+1,Nx+1)=0;
Fxz1(Nz+1,Nx+1)=0;
Fxy1(Nz+1,Nx+1)=0;
Fxy2(Nz+1,Nx+1)=0;

Sxx1(Nz+1,Nx+1)=0;
Sxx2(Nz+1,Nx+1)=0;
Syy1(Nz+1,Nx+1)=0;
Syy2(Nz+1,Nx+1)=0;
Szz1(Nz+1,Nx+1)=0;
Syz1(Nz+1,Nx+1)=0;
Sxz1(Nz+1,Nx+1)=0;
Sxy1(Nz+1,Nx+1)=0;
Sxy2(Nz+1,Nx+1)=0;

T(Nz+1,Nx+1)=0;

xi=1;
for x = x_min:x_step:x_max
   zi=1;
   for z = z_min: z_step: z_max
      Fxx1(zi,xi)=fxx1(x,0,z);
      Fxx2(zi,xi)=fxx2(x,0,z);
      Fyy1(zi,xi)=fyy1(x,0,z);
      Fyy2(zi,xi)=fyy2(x,0,z);
      Fzz1(zi,xi)=fzz1(x,0,z);
      Fyz1(zi,xi)=fyz1(x,0,z);
      Fxz1(zi,xi)=fxz1(x,0,z);
      Fxy1(zi,xi)=fxy1(x,0,z);
      Fxy2(zi,xi)=fxy2(x,0,z);

      Sxx1(zi,xi)=sxx1(x,0,z);
      Sxx2(zi,xi)=sxx2(x,0,z);
      Syy1(zi,xi)=syy1(x,0,z);
      Syy2(zi,xi)=syy2(x,0,z);
      Szz1(zi,xi)=szz1(x,0,z);
      Syz1(zi,xi)=syz1(x,0,z);
      Sxz1(zi,xi)=sxz1(x,0,z);
      Sxy1(zi,xi)=fxy1(x,0,z);
      Sxy2(zi,xi)=fxy2(x,0,z);

      zi=zi+1;
   end
   xi=xi+1;
end

%------------Calculating the V-E terms-------------------------%
% -------------- Relaxation function
t_ve_sample = 0.001;
t_relax_total = t_total;
t_ve = 0:t_ve_sample:t_relax_total;
N_ve = t_relax_total/t_ve_sample;
m1 = 1;
m2 = 0.8;
n1 = 0.5;
n2 = 0.2;
V1(1) = m1/n1;
V1(N_ve+1) = 0;
V2 = m1/n1*(m2/m1-n2/n1).*exp(-n2/n1.*t_ve);
V = V1 + V2;

% ------------- Load Profile
% theta = pi/3;
% Mag_Pn =
% Mag_Pt =
P_mag = 1; %N/m2
P_freq = 0.5; %Hz
P_period = 1/P_freq;
t_p_sample = 0.0001;
t_p = 0:t_p_sample:P_period;
P = P_mag + P_mag .* cos(2*pi*P_freq.*t_p-pi);

% ------------- Convolution
P_V = conv(P,V).*t_ve_sample;
% Show loads, relaxation and convolution results
figure;
subplot(2,2,1);plot(P);
subplot(2,2,2);plot(V);
subplot(2,2,3);plot(P_V);
saveas(gcf,'convolution','fig');

% ------------- Dynamic Stress
mkdir ('xoz');
cd ('xoz');

for t_current = 0:t_step:t_total

   dir_name = ['t=',num2str(t_current),'s'];
   mkdir (dir_name);
   cd (dir_name);

   % Calculate the stress at this interval
   Nt = ceil(t_current/t_ve_sample) + 1;
   E_term = P(Nt);
   VE_term = P_V(Nt);

   % Boussinesq's stress field (due to vertical load)
   DFxx = E_term * Fxx1 * cos(angle) + VE_term *
cos(angle)* Fxx2 ;
   DFyy = E_term * Fyy1 * cos(angle) + VE_term *
cos(angle)* Fyy2 ;
   DFzz = E_term * Fzz1 * cos(angle);
   DFyz = E_term * Fyz1 * cos(angle);
   DFxz = E_term * Fxz1 * cos(angle);
   DFxy = E_term * Fxy1 * cos(angle)+ VE_term *
cos(angle)* Fxy2 ;

   % Cerruti's stress field (due to tangential load)
   DSxx = E_term * Sxx1 * sin(angle)+ VE_term *
sin(angle)* Sxx2 ;
   DSyy = E_term * Syy1 * sin(angle)+ VE_term *
sin(angle)* Syy2 ;
   DSzz = E_term * Szz1 * sin(angle);
   DSyz = E_term * Syz1 * sin(angle);
   DSxz = E_term * Sxz1 * sin(angle);
```

```
    DSxy = E_term * Sxy1 * sin(angle)+ VE_term *
sin(angle)* Sxy2 ;

    % Total stress field
    DTxx = DFxx + DSxx;
    DTyy = DFyy + DSyy;
    DTzz = DFzz + DSzz;
    DTyz = DFyz + DSyz;
    DTxz = DFxz + DSxz;
    DTxy = DFxy + DSxy;

    % Save the results at this interval
    %------------------------------------------------------------------
    if t_current~=0

    figure;
    contour(xx,zz,DTxx);set(gca,'YDir','reverse');
    grid on; colorbar;
    xlabel('x(m)');ylabel('depth z(m)');ylim([0 z_max]);
    filename = ['DTxx at t=',num2str(t_current)];
    title(filename);
    saveas(gcf,filename,'fig');

    figure;
    contour(xx,zz,DTyy,ct);set(gca,'YDir','reverse');
    grid on; colorbar;
    xlabel('x(m)');ylabel('depth z(m)');ylim([0 z_max]);
    filename = ['DTyy at t=',num2str(t_current)];
    title(filename);
    saveas(gcf,filename,'fig');

    figure;
    contour(xx,zz,DTzz);set(gca,'YDir','reverse');
    xlabel('x(m)');ylabel('depth z(m)');ylim([0 z_max]);
    grid on; colorbar;
    filename = ['DTzz at t=',num2str(t_current)];
    title(filename);
    saveas(gcf,filename,'fig');

    figure;
    contour(xx,zz,DTyz);set(gca,'YDir','reverse');
    xlabel('x(m)');ylabel('depth z(m)');ylim([0 z_max]);
    grid on; colorbar;
    title(filename);
    filename = ['DTyz at t=',num2str(t_current)];
    saveas(gcf,filename,'fig');

    figure;
    contour(xx,zz,DTxz);set(gca,'YDir','reverse');
    xlabel('x(m)');ylabel('depth z(m)');ylim([0 z_max]);
    grid on; colorbar;
    filename = ['DTxz at t=',num2str(t_current)];
    title(filename);
    saveas(gcf,filename,'fig');

    figure;
    contour(xx,zz,DTxy);set(gca,'YDir','reverse');
    xlabel('x(m)');ylabel('depth z(m)');ylim([0 z_max]);
    grid on; colorbar;
    filename = ['DTxy at t=',num2str(t_current)];
    title(filename);
    saveas(gcf,filename,'fig');

    close ALL;
    %------------------------------------------------------------------


    % Calculate the principal stress at this interval
    xi=1;
    for x = x_min:x_step:x_max
        zi=1;
        for z = z_min: z_step: z_max
            S =
[DTxx(zi,xi),DTxy(zi,xi),DTxz(zi,xi);DTxy(zi,xi),DTyy(zi,xi
),DTyz(zi,xi);DTxz(zi,xi),DTyz(zi,xi),DTzz(zi,xi)];
            V = eig(S);
            s1 = abs(V(1)); s2 = abs(V(2)); s3 = abs(V(3));
            ss = [s1,s2,s3];
            s_tresce = 0.5*max(ss);
            T(zi,xi) = s_tresce;
            zi=zi+1;
        end
        xi=xi+1;
    end
    % Save results at this interval

    figure;
    contour(xx,zz,T);set(gca,'YDir','reverse');
    grid on; colorbar;
    xlabel('x(m)');ylabel('depth z(m)');
    filename = ['Treca stress',num2str(t_current)];
    title(filename);
    saveas(gcf,filename,'fig');
    close ALL;
    end
    save workspace
    cd ..
end
cd ..

end % end function
```

```
This function calculates all stress components on yoz plane
and generate the plots
************************************************
function plot_yoz(x_value, y_min, y_step, y_max, z_min,
z_step, z_max, t_step, angle)
% Entries are the boundaries of y and z
% z_min cannot be 0, or "divided by 0" will occur
% x needs to set

global t_total
x = x_value;
ct = 30; % number of contours
Ny = ceil((y_max - y_min)/(y_step));
Nz = ceil((z_max - z_min)/(z_step));
[yy,zz] = meshgrid(y_min:y_step:y_max,
z_min:z_step:z_max);

%------------Calculating the spatial terms--------------------%
% Initialization
Fxx1(Nz+1,Ny+1)=0;
Fxx2(Nz+1,Ny+1)=0;
Fyy1(Nz+1,Ny+1)=0;
Fyy2(Nz+1,Ny+1)=0;
Fzz1(Nz+1,Ny+1)=0;
Fyz1(Nz+1,Ny+1)=0;
Fxz1(Nz+1,Ny+1)=0;
Fxy1(Nz+1,Ny+1)=0;
Fxy2(Nz+1,Ny+1)=0;

Sxx1(Nz+1,Ny+1)=0;
Sxx2(Nz+1,Ny+1)=0;
Syy1(Nz+1,Ny+1)=0;
Syy2(Nz+1,Ny+1)=0;
Szz1(Nz+1,Ny+1)=0;
Syz1(Nz+1,Ny+1)=0;
Sxz1(Nz+1,Ny+1)=0;
Sxy1(Nz+1,Ny+1)=0;
Sxy2(Nz+1,Ny+1)=0;

T(Nz+1,Ny+1)=0;

yi=1;
for y = y_min:y_step:y_max
   zi=1;
   for z = z_min: z_step: z_max
      Fxx1(zi,yi)=fxx1(x,y,z);
      Fxx2(zi,yi)=fxx2(x,y,z);
      Fyy1(zi,yi)=fyy1(x,y,z);
      Fyy2(zi,yi)=fyy2(x,y,z);
      Fzz1(zi,yi)=fzz1(x,y,z);
      Fyz1(zi,yi)=fyz1(x,y,z);
      Fxz1(zi,yi)=fxz1(x,y,z);
      Fxy1(zi,yi)=fxy1(x,y,z);
      Fxy2(zi,yi)=fxy2(x,y,z);

      Sxx1(zi,yi)=sxx1(x,y,z);
      Sxx2(zi,yi)=sxx2(x,y,z);
      Syy1(zi,yi)=syy1(x,y,z);
      Syy2(zi,yi)=syy2(x,y,z);
      Szz1(zi,yi)=szz1(x,y,z);
      Syz1(zi,yi)=syz1(x,y,z);
      Sxz1(zi,yi)=sxz1(x,y,z);
      Sxy1(zi,yi)=fxy1(x,y,z);
      Sxy2(zi,yi)=fxy2(x,y,z);

      zi=zi+1;
   end
   yi=yi+1;
end

%------------Calculating the convolution--------------------------%
% -------------- Relaxation function
t_ve_sample = 0.001;
t_relax_total = t_total;
t_ve = 0:t_ve_sample:t_relax_total;
N_ve = t_relax_total/t_ve_sample;
m1 = 1;
m2 = 0.8;
n1 = 0.5;
n2 = 0.2;
V1(1) = m1/n1;
V1(N_ve+1) = 0;
V2 = m1/n1*(m2/m1-n2/n1).*exp(-n2/n1.*t_ve);
V = V1 + V2;

% ------------- Load Profile
% theta = pi/3;
% Mag_Pn =
% Mag_Pt =
P_mag = 1;
P_freq = 0.5; %Hz
P_period = 1/P_freq;
t_p_sample = 0.0001;
t_p = 0:t_p_sample:P_period;
P = P_mag + P_mag .* cos(2*pi*P_freq.*t_p-pi);

% ------------- Convolution
P_V = conv(P,V).*t_ve_sample;
% Show loads, relaxation and convolution results
figure;
subplot(2,2,1);plot(P);
subplot(2,2,2);plot(V);
subplot(2,2,3);plot(P_V);

% ------------- Calculating Dynamic Stress-----------------------
mkdir ('yoz');
cd ('yoz');

for t_current = 0:t_step:t_total
   dir_name = ['t=',num2str(t_current),'s'];
   mkdir (dir_name);
   cd (dir_name);

   % Calculate the stress at this interval
   Nt = ceil(t_current/t_ve_sample) + 1;
   E_term = P(Nt);
   VE_term = P_V(Nt);

   % Boussinesq's stress field (due to vertical load)
   DFxx = E_term * Fxx1 * cos(angle) + VE_term *
cos(angle)* Fxx2 ;
   DFyy = E_term * Fyy1 * cos(angle) + VE_term *
cos(angle)* Fyy2 ;
   DFzz = E_term * Fzz1 * cos(angle);
   DFyz = E_term * Fyz1 * cos(angle);
   DFxz = E_term * Fxz1 * cos(angle);
   DFxy = E_term * Fxy1 * cos(angle)+ VE_term *
cos(angle)* Fxy2 ;

   % Cerruti's stress field (due to tangential load)
   DSxx = E_term * Sxx1 * sin(angle)+ VE_term *
sin(angle)* Sxx2 ;
   DSyy = E_term * Syy1 * sin(angle)+ VE_term *
sin(angle)* Syy2 ;
   DSzz = E_term * Szz1 * sin(angle);
   DSyz = E_term * Syz1 * sin(angle);
   DSxz = E_term * Sxz1 * sin(angle);
   DSxy = E_term * Sxy1 * sin(angle)+ VE_term *
sin(angle)* Sxy2 ;
   % Total stress field
```

```
    DTxx = DFxx + DSxx;
    DTyy = DFyy + DSyy;
    DTzz = DFzz + DSzz;
    DTyz = DFyz + DSyz;
    DTxz = DFxz + DSxz;
    DTxy = DFxy + DSxy;

    % Save the results at this interval
    %-----------------------------------------------
    figure;
    contour(yy,zz,DTxx,ct);set(gca,'YDir','reverse');
    grid on; colorbar;
    filename = ['DTxx at t=',num2str(t_current)];
    xlabel('y(m)');ylabel('depth z(m)');ylim([0 z_max]);
    title(filename);
    saveas(gcf,filename,'fig');

    figure;
    contour(yy,zz,DTyy,ct);set(gca,'YDir','reverse');
    grid on; colorbar;
    xlabel('y(m)');ylabel('depth z(m)');ylim([0 z_max]);
    filename = ['DTyy at t=',num2str(t_current)];
    title(filename);
    saveas(gcf,filename,'fig');

    figure;
    contour(yy,zz,DTzz,ct);set(gca,'YDir','reverse');
    grid on; colorbar;
    xlabel('y(m)');ylabel('depth z(m)');ylim([0 z_max]);
    filename = ['DTzz at t=',num2str(t_current)];
    title(filename);
    saveas(gcf,filename,'fig');

    figure;
    contour(yy,zz,DTyz,ct);set(gca,'YDir','reverse');
    grid on; colorbar;
    xlabel('y(m)');ylabel('depth z(m)');ylim([0 z_max]);
    filename = ['DTyz at t=',num2str(t_current)];
    title(filename);
    saveas(gcf,filename,'fig');

    figure;
    contour(yy,zz,DTxz,ct);set(gca,'YDir','reverse');
    grid on; colorbar;
    xlabel('y(m)');ylabel('depth z(m)');ylim([0 z_max]);
    filename = ['DTxz at t=',num2str(t_current)];
    title(filename);
    saveas(gcf,filename,'fig');

    figure;
    contour(yy,zz,DTxy,ct);set(gca,'YDir','reverse');
    grid on; colorbar;
    xlabel('y(m)');ylabel('depth z(m)');ylim([0 z_max]);
    filename = ['DTxy at t=',num2str(t_current)];
    title(filename);
    saveas(gcf,filename,'fig');

    close ALL;
    %-----------------------------------------------
    % Calculate the principal stress at this interval
    yi=1;
    for y = y_min:y_step:y_max
        zi=1;
        for z = z_min: z_step: z_max
            S =
[DTxx(zi,yi),DTxy(zi,yi),DTxz(zi,yi);DTxy(zi,yi),DTyy(zi,yi
),DTyz(zi,yi);DTxz(zi,yi),DTyz(zi,yi),DTzz(zi,yi)];
            V = eig(S);
            s1 = abs(V(1)); s2 = abs(V(2)); s3 = abs(V(3));
            ss = [s1,s2,s3];
            s_tresce = 0.5*max(ss);
            T(zi,yi) = s_tresce;

            zi=zi+1;
        end
        yi=yi+1;
    end
    % Save results at this interval

    figure;
    contour(yy,zz,T);set(gca,'YDir','reverse');
    grid on; colorbar;
    filename = ['Treca stress',num2str(t_current)];
    xlabel('y(m)');ylabel('depth z(m)');ylim([0 z_max]);
    title(filename);
    saveas(gcf,filename,'fig');
    close ALL;
    save workspace
    cd ..
end
cd ..

end % end function
```

These are the codes to run in MATLAB command window for initiation and results calculation

****

```
clear
global a b t_total
a=0.1; b=0.001; t_total=1;
t_step = 1;
angle = pi/6;

x_value = 0;
y_min  =  -0.0018;
y_max  =  0.0018;
y_step =  0.0009;
z_max  = 0.000401;
z_min  = 0.000001;
z_step = 0.0002;

plot_yoz(x_value, y_min, y_step, y_max, z_min, z_step,
z_max, t_step, angle);

plot_xoz (x_min, x_step, x_max, z_min, z_step, z_max,
t_step, angle);
```